4. EXPLANATORY NOTES[1]

Shipboard Scientific Party[2]

INTRODUCTION

In this chapter, we have assembled information that will help the reader understand the observations on which our preliminary conclusions are based and also help the interested investigator select samples and data for further analysis. This information concerns shipboard operations and analyses described in the site reports in the *Initial Reports* volume of the Leg 166 *Proceedings of the Ocean Drilling Program.* Methods used by various investigators for shore-based analyses of Leg 166 data will be described in the individual scientific contributions to be published in the *Scientific Results* volume.

Authorship of Site Chapters

The separate sections of the site chapters were written by the following shipboard scientists (authors are listed in alphabetical order, no seniority is implied):

Site Summary: Eberli, Swart
Background and Objectives: Eberli, Swart
Operations: Malone, Pollard
Lithostratigraphy: Arai, Bernet, Betzler, Déjardin, Emmanuel, Frank, Haddad, Reijmer
Biostratigraphy: Katz, Kroon, Sato, Wright
Paleomagnetism: McNeill, Montgomery
Composite Sections: Christensen
Organic Geochemistry: Schlovsbo
Inorganic Geochemistry: De Carlo, Kramer
Physical Properties: Anselmetti, Isern, Kenter, Nagihara
Downhole Logging: McKenzie, Pirmez, Williams
Seismic Stratigraphy: Anselmetti, Eberli
In Situ Temperature Measurements: Nagihara
Summary and Conclusions: Eberli, Swart

Shipboard Scientific Procedures

Core handling and shipboard scientific procedures, including the numbering of sites, holes, cores, sections, and samples, were similar to those reported in previous *Initial Reports* volumes of the *Proceedings of the Ocean Drilling Program* (e.g., Shipboard Scientific Party, 1995a).

At the end of the leg, the cores were transferred from the ship in refrigerated airfreight containers to cold storage at the Bremen Core Repository of the Ocean Drilling Program, at the University of Bremen, Federal Republic of Germany.

LITHOSTRATIGRAPHY

Sediment Core Description Forms

The sediment core description forms, or barrel sheets, summarize the data obtained during shipboard analysis of each core. The ODP conventions used for the compilation of each part of the core description forms and the exceptions to these procedures adopted by the Leg 166 Shipboard Scientific Party are described below.

Graphic Lithology Column

A slightly modified version of the lithologic classification of Mazzullo et al. (1988) into (I) granular and (II) chemical sediment and rocks was used during Leg 166. The classification adopted is outlined in the "Sediment and Rock Classification" section of this chapter. The only significant modification is a further subdivision of calcareous sediment into pelagic and nonpelagic. Sediment type is represented graphically on the core description forms using the symbols illustrated in Figure 1.

In the "Graphic Lithology" column, a maximum of three different lithologies (for interbedded sediments) or three different components (for mixed sediments) can be represented within the same core interval. Percentages are rounded to the nearest 10%, and only lithologies that constitute at least 10% of the core are shown. Only lithologic units that are 20 cm or greater in thickness can be portrayed in this column. Minor lithologies present as thin interbeds within the major lithology are shown by a dashed vertical line dividing the lithologies. Components present as minor fractions of the main lithology are shown by a continuous vertical line. All core photographs and graphic lithology columns are included in Section 3 of this volume.

Sedimentary Structures

The location and nature of sedimentary structures in the cores are shown in the "Structure" column of the core description form. The symbols used to designate the structures found in Leg 166 cores are shown in Figure 2.

Sediment Disturbance

Observations of drilling-related disturbance over an interval of 20 cm or more are recorded in the "Disturbance" column using the symbols shown in Figure 2. The degree of drilling disturbance is described for soft and firm sediments using the following categories.

1. Slightly disturbed: bedding contacts are slightly deformed.
2. Moderately disturbed: bedding contacts have undergone extreme bowing.
3. Highly disturbed: bedding is completely deformed as flow-in, coring/drilling slough, and other soft sediment stretching and/or compressional shearing structures attributed to the coring/drilling.
4. Soupy: intervals are water-saturated and have lost all aspects of original bedding.

[1]Eberli, G.P., Swart, P.K., Malone, M.J., et al., 1997. *Proc. ODP, Init. Repts.*, 166: College Station, TX (Ocean Drilling Program).
[2]Shipboard Scientific Party is given in the list preceding the Table of Contents.

Previous Chapter Table of Contents Next Chapter

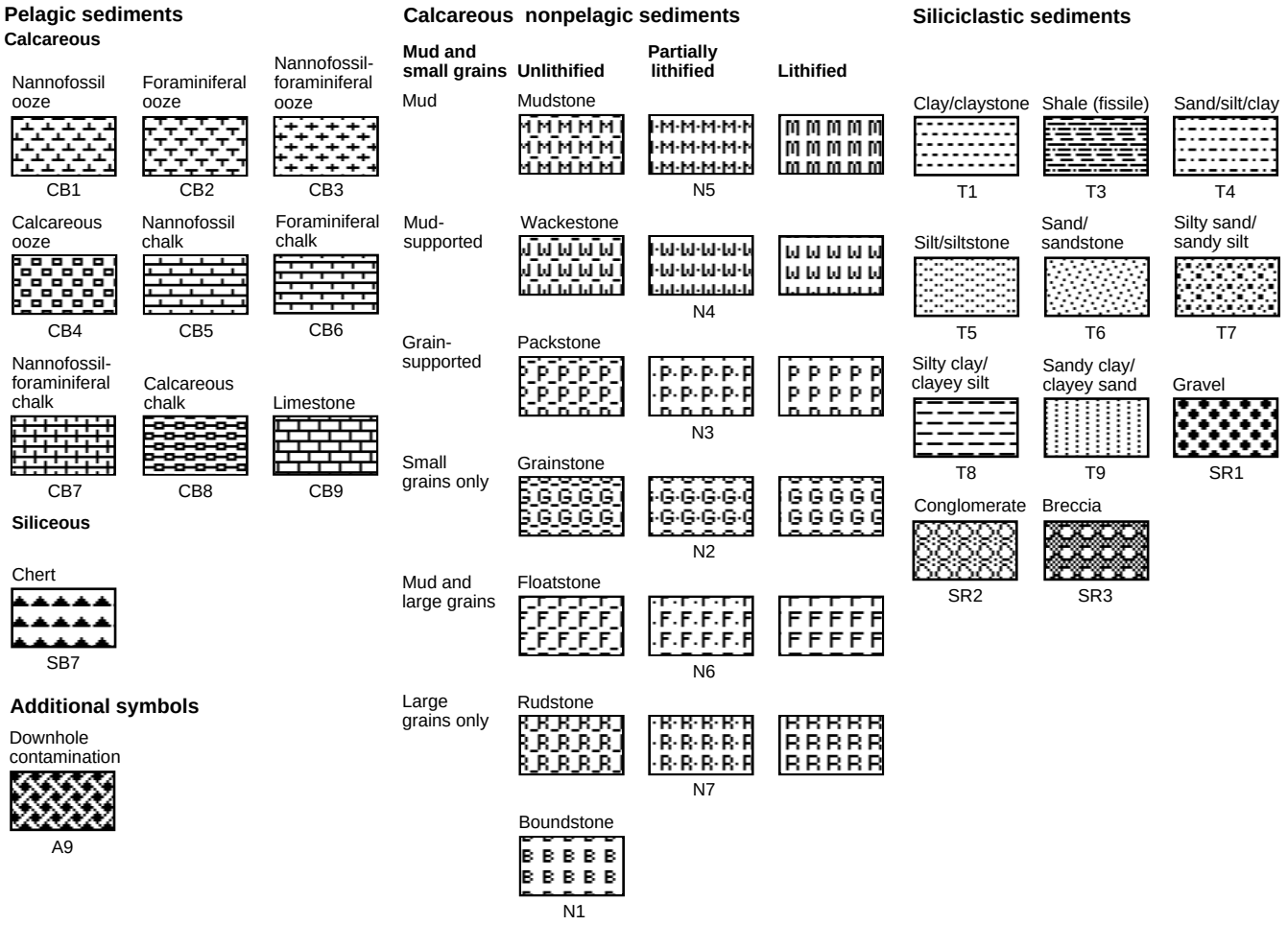

Figure 1. Key to lithologic symbols used in graphic lithology column on core description forms.

The degree of fracturing in indurated sediments and rocks is described using the following categories.

1. Slightly fractured: core pieces are in place and broken.
2. Moderately fractured: core pieces are in place or partly displaced, and original orientation is preserved or recognizable (drilling slurry may surround fragments, i.e. drilling/coring "biscuits" are evident).
3. Highly fractured: core pieces are probably in correct stratigraphic sequence (although they may not represent the entire sequence), but original orientation is lost.
4. Drilling breccia: the core is crushed and broken into many small and angular pieces, with original orientation and stratigraphic position lost; often drilling breccia is completely mixed with drilling slurry.

Samples

The positions of samples taken from each core for analysis are indicated by letters in the "Sample" column of the core description form as follows: S (smear slide), T (thin section), M (micropaleontology), I (interstitial water), and B (micropaleontology thin section).

Color

After the core was split, color was determined using a Minolta CM-2002 hand-held spectrophotometer. These measurements were determined on the damp core surface, and Glad brand clear plastic film was used to cover the core. The Minolta CM-2002 measures reflected visible light in thirty-one 10-nm-wide bands ranging from 400 to 700 nm. Colors determined by this method correspond to those of the Munsell Color Company (1992). Routine measurements were made at evenly spaced intervals of each section, taking into account section length and the position of voids within the section. The measurement spacing was occasionally reduced below 10 cm for core intervals with distinct color variations or changes in lithology over short distances.

Before and after obtaining measurements from each core, the spectrophotometer was calibrated for white color reflectance by attaching its white calibration cap. In addition, instrument calibration was checked using a white barium-sulfate plate, which is the standard used for calibrating laboratory-grade spectrophotometers. These white color calibrations were made to avoid variation in color readings dependent on the laboratory environment (temperature, humidity, and background light) and instrument deviations. Spectrophotometer readings were recorded using the Spectrolog Version 3.0.

Lithologic Description

Core description forms were prepared and consist of a list of major lithologies followed by a more detailed description of the composition (as determined from smear slides), color, sedimentary structures, and other notable features. Descriptions and locations of thin, interbedded, or minor lithologies are also included in the text. The

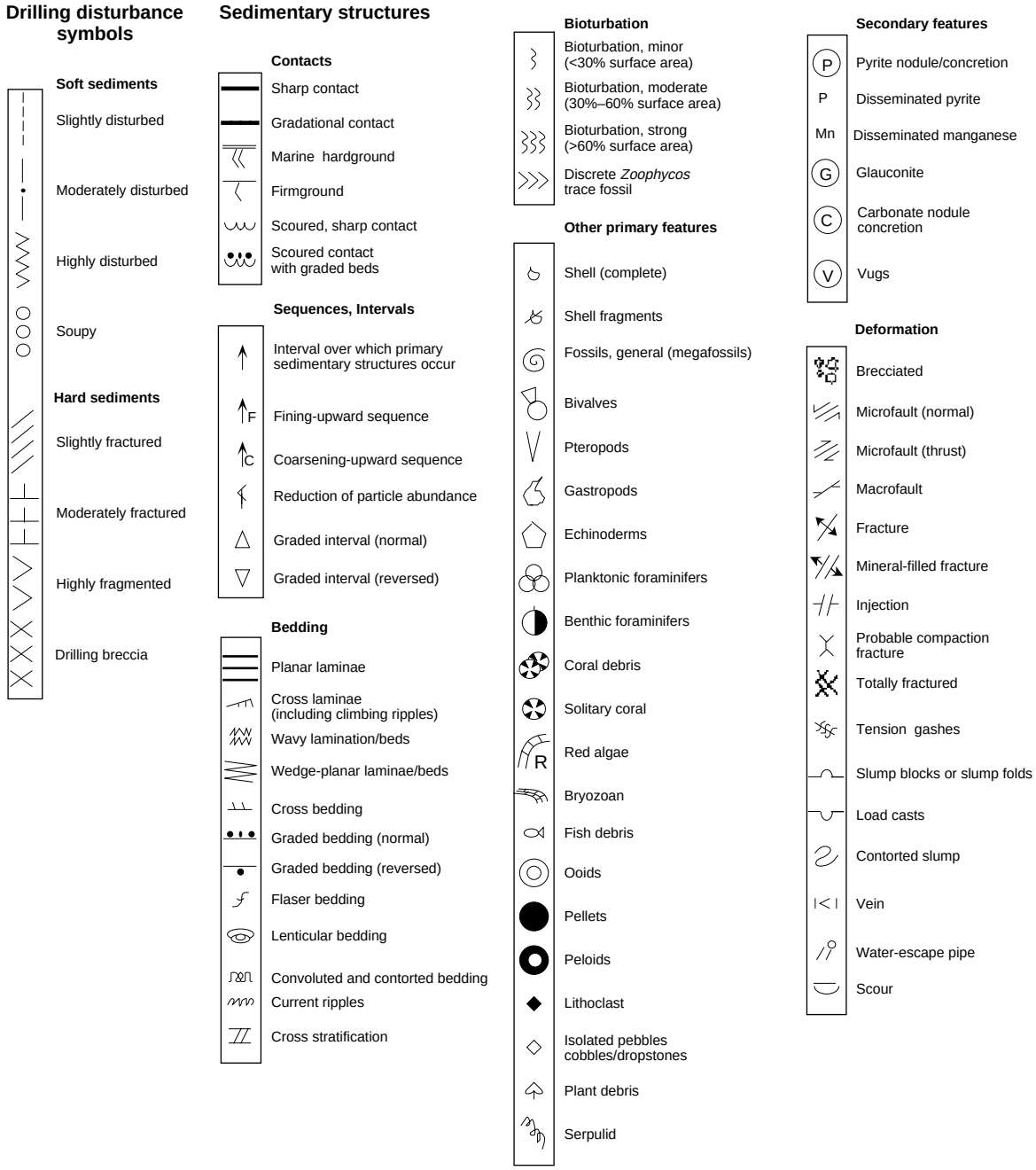

Figure 2. Symbols showing drilling disturbance and sedimentary structures used for core descriptions.

terminology for the thickness of sedimentary beds and laminae follows McKee and Weir (1953): very thick bedded (>100 cm), thick bedded (30–100 cm), medium bedded (10–30 cm), thin bedded (3–10 cm), thickly laminated (>0.3 cm) and thinly laminated (<0.3 cm). The term "wispy lamination" was used to describe laminae with undulatory and anastomosing shapes.

Smear Slides and Thin Sections

Tables summarizing data from smear-slide and thin-section analyses are included in Sections 4 and 5 and on CD-ROM in the back of this volume. These tables include information about the sample location, whether the sample represents a dominant (D) or a minor (M) lithology in the core, and the estimated percentages of sand, silt, and clay, together with all identified components.

Sediment and Rock Classification

Grain Types

Grain types in granular sediments and rocks were classified according to depositional origin and mineralogy: (1) pelagic calcareous, (2) pelagic siliceous, (3) nonpelagic calcareous, and (4) siliciclastic particles. Their definitions are as follows.

1. Pelagic grains are fine-grained skeletal debris produced within the upper part of the water column in open-marine environments by:
   a. Calcareous microfauna and microflora (foraminifers, pteropods, and nannofossils and associated organisms), and

   b. Siliceous microfauna and microflora (radiolarians, and diatoms and associated organisms).
2. Nonpelagic grains are coarse- to fine-grained particles deposited in hemipelagic and periplatform environments and consist of the following.
   a. Calcareous skeletal and nonskeletal grains and fragments (e.g., bioclasts, peloids, micrite). Note that the term micrite is used to define very fine calcareous particles (<4 µm) of indeterminate origin. Such particles can be either recrystallized nannofossils or nonpelagic bank-derived calcareous mud in pelagic lithologies.
   b. Siliceous clastic grains comprising minerals and rock fragments that were eroded from plutonic, sedimentary, and metamorphic rocks.
   c. Siliceous clastic grains comprising glass shards, rock fragments, and mineral crystals that were produced by volcanic processes.

Granular Sediment and Rock Classification Scheme

Variations in the relative proportions of the five grain types described above define four major classes of granular sediments and rocks: (1) calcareous and siliceous pelagic, (2) nonpelagic calcareous, (3) siliciclastic, and (4) mixed.

Pelagic sediments and rocks contain 60% or more pelagic grains and 40% or less nonpelagic calcareous and siliciclastic grains. *Nonpelagic calcareous sediments and rocks* include 60% or more nonpelagic calcareous grains and 40% or less pelagic plus nonpelagic siliciclastic grains. *Siliciclastic sediments and rocks* are composed of 60% or more siliciclastic grains and 40% or less pelagic plus nonpelagic calcareous grains. *Mixed sediments and rocks* are composed of 40%–60% nonpelagic calcareous and siliciclastic grains, and 40%–60% calcareous plus siliceous pelagic grains.

Principal Names

Sediments and rocks were named solely on the basis of composition and texture. Within each class, granular sediments and rocks were classified using a principal name and major and minor modifiers. Principal names define the degree of consolidation (firmness) and granular-sediment class. Composition is the most important classifier for pelagic and siliciclastic sediments and rocks (Table 1), whereas texture is more significant for the classification of nonpelagic calcareous sediments and rocks (Table 2). Compositions and textures of cored sediments and rocks were determined aboard ship by (1) unaided visual observation, (2) visual observation using a hand lens, and (3) visual estimates in smear slides, thin sections, and coarse fractions with the aid of a microscope. Calcium carbonate content was qualitatively estimated in smear slides and quantitatively by coulometric analysis (see "Organic Geochemistry" section, this chapter).

Firmness

Firmness of recovered materials was defined as in Gealy et al. (1971). Three classes of firmness were used to describe calcareous sediments and rocks.

1. Unlithified: soft sediments that have little strength and are readily deformed under the pressure of a fingernail or the broad blade of a spatula. This corresponds to the term *ooze* for pelagic calcareous sediments. In nonpelagic calcareous sediments the prefix *unlithified* is used (e.g., *unlithified packstone*).
2. Partly lithified: firm but friable sediments that can be scratched with a fingernail or the edge of a spatula blade. The term *chalk* is used for firm or friable pelagic calcareous material. In nonpelagic calcareous sediment the prefix *partially lithified* is used (e.g., *partially lithified grainstone*).
3. Lithified: hard, nonfriable cemented rock, difficult or impossible to scratch with a fingernail or the edge of a spatula. The term *limestone* (lithified ooze) is used for pelagic calcareous material. In nonpelagic calcareous material a modified Dunham (1962) classification (described below) is used.

Two classes of firmness were used to describe *siliceous sediments and rocks:*

Table 1. Lithologic description of granular sediments and rocks, including major and minor modifiers.

Sediment class	Major modifiers	Principal names	Minor modifiers
Pelagic sediment	Composition of pelagic and NPC grains present in major amounts. Texture of clastic grains present in major amounts.	Ooze Chalk Limestone Chert	Composition of pelagic and NPC grains present in minor amounts. Texture of clastic grains present in minor amounts.
Siliciclastic sediment	Composition of all grains present in major amounts. Grain fabric (gravels only). Grain shape (optional). Sediment color (optional).	Gravel Sand Silt Clay, etc.	Composition of all grains present in minor amounts. Texture and composition of siliciclastic grains present as matrix (for coarse-grained clastic sediments).
Mixed sediment	Composition of NPC and pelagic grains present in major amounts. Texture of clastic grains present in major amounts.	Mixed sediments	Composition of NPC and pelagic grains present in minor amounts. Texture of clastic grains present in minor amounts.

Note: NPC = nonpelagic carbonate.

Table 2. Lithologic description of nonpelagic calcareous sediments and rocks, including the major modifiers.

Sediment class	Major modifiers	Names
Nonpelagic sediment	Texture Hydrodynamically accumulated or primary biogenic in situ formation Degree of lithification	Mudstone, partially lithified mudstone, unlithified mudstone Wackestone, partially lithified wackestone, unlithified wackestone Packstone, partially lithified packstone, unlithified packstone Grainstone, partially lithified grainstone, unlithified grainstone Floatstone, partially lithified floatstone, unlithified floatstone Rudstone, partially lithified rudstone, unlithified rudstone Boundstone

1. Soft: sediment core can be split with a wire cutter. Soft terrigenous sediment, pelagic clay, and transitional calcareous sediments are termed sand, silt, or clay.
2. Hard: the core is hard (i.e., consolidated or well indurated) if it must be cut with a hand or diamond saw. For these materials, the suffix *stone* is added to the soft-sediment name (e.g., sandstone, siltstone, and claystone). Note that this varies from terms used to described nonpelagic calcareous sediments, for which the suffix *stone* has no firmness implications.

Pelagic Sediments and Rocks

Principal names used to describe pelagic sediments and rocks during Leg 166 are as follows:

1. *Pelagic clay:* unconsolidated authigenic pelagic material (>15%) and siliceous pelagic sediment (lithified examples are termed pelagic claystone);
2. *Ooze:* unconsolidated calcareous and/or siliceous pelagic sediment;
3. *Chalk:* firm pelagic sediment composed predominantly of calcareous pelagic grains;
4. *Limestone:* hard pelagic sediment composed predominantly of calcareous pelagic grains; and
5. *Chert:* vitreous or lustrous, conchoidally fractured, highly indurated rock composed predominantly of authigenic silica.

Nonpelagic Calcareous Sediments and Rocks

Nonpelagic calcareous sediments and rocks were classified using a modification of the original Dunham (1962) classification in conjunction with depositional textures described by Embry and Klovan (1971; Fig. 3):

1. *Mudstone:* mud-supported fabric, with less than 10% grains, grains <2 mm in size;
2. *Wackestone:* mud-supported fabric, with greater than 10% grains, grains <2 mm in size;
3. *Packstone:* grain-supported fabric, with intergranular mud, grains <2 mm in size;
4. *Grainstone:* grain-supported fabric, no mud, grains <2 mm in size;
5. *Floatstone:* matrix-supported fabric, grains >2 mm in size;
6. *Rudstone:* grain-supported fabric, grains >2 mm in size;
7. *Boundstone:* components organically bound during deposition;
8. *Bafflestone:* formed by organisms that act as baffles;
9. *Bindstone:* formed by organisms that encrust and bind; and
10. *Framestone:* formed by organisms that build a rigid framework.

Mixed Pelagic and Nonpelagic Calcareous Sediments and Rocks

Sediments and rocks that consist of a mixture of pelagic and nonpelagic calcareous grains and contain aragonite and/or magnesian calcite (confirmed by X-ray diffraction analysis) were (1) described lithologically using the classification scheme explained above for nonpelagic calcareous sediments and rocks, and (2) labeled additionally as *periplatform oozes* and *periplatform chalks* (e.g., Schlager and James, 1978).

Siliciclastic Sediments and Rocks

For siliciclastic sediments and rocks, texture is the main criterion for the selection of a principal name. The Udden-Wentworth grain-size scale (Fig. 4; Wentworth, 1922) defines the grain-size ranges and the names of the textural groups (*gravel*, *sand*, *silt*, and *clay*) and subgroups (*fine sand*, *coarse silt*, etc.). When two or more textural groups or subgroups are present, the principal names appear in order of increasing abundance. Eight major textural categories can be defined on the basis of the relative proportions of sand, silt, and clay (Fig. 5). Distinguishing between some size categories is difficult (e.g., silty clay and clayey silt) without accurate measurements of weight percentages. The terms *conglomerate* and *breccia* are the principal names of gravels with well-rounded and angular clasts, respectively.

Mixed Sediments and Rocks

For mixed sediments and rocks, the principal name describes the degree of lithification, with the term *mixed sediments* used for unlithified sediment, and the term *mixed sedimentary rock* used for lithified sediment.

Major and Minor Modifiers

To describe the lithology of the granular sediments and rocks in greater detail, the principal name of a granular-sediment class is preceded by major modifiers and followed by minor modifiers (Table 1). Minor modifiers are preceded by the term "with." The most common uses of major and minor modifiers are to describe the composition and textures of grain types that are present in major (25%–40%) and minor (10%–25%) proportions. In addition, major modifiers can be used to describe grain fabric, grain shape, and sediment color.

The composition of pelagic grains can be described in greater detail with the major and minor modifiers *nannofossil*, *foraminifer*, *calcareous*, and *siliceous.* The terms *calcareous* and *siliceous* are used

<table>
<tr><td colspan="6">Allochthonous limestones:
original components not organically
bound during deposition</td><td colspan="3">Autochthonous limestones:
original components organically
bound during deposition</td></tr>
<tr><td colspan="4">Less than 10% >2-mm components</td><td colspan="2">Greater than
10% >2-mm
components</td><td colspan="3">Boundstone</td></tr>
<tr><td colspan="3">Contains lime mud (<0.03 mm)</td><td>No
lime
mud</td><td rowspan="2">Matrix
supported</td><td rowspan="2">>2-mm
grain
supported</td><td rowspan="3">By
organisms
that
act as
barriers</td><td rowspan="3">By
organisms
that
encrust
and
bind</td><td rowspan="3">By
organisms
that
build
a rigid
framework</td></tr>
<tr><td colspan="2">Mud supported</td><td colspan="2" rowspan="2">Grain
supported</td></tr>
<tr><td>Less than
10% grains
(>0.03 mm
to <2 mm)</td><td>Greater
than
10%
grains</td><td></td><td></td></tr>
<tr><td>Mudstone</td><td>Wackestone</td><td>Packstone</td><td>Grainstone</td><td>Floatstone</td><td>Rudstone</td><td>Bafflestone</td><td>Bindstone</td><td>Framestone</td></tr>
</table>

Figure 3. The Dunham (1962) classification of limestones according to depositional texture, as modified by Embry and Klovan (1971).

Millimeters (mm)	Micrometers (μm)	Phi (f)	Wentworth size class	
4096		–12.0	Boulder	
256		–8.0	Cobble	Gravel
64		–6.0	Pebble	
4		–2.0	Granule	
2.00		–1.0	Very coarse sand	
1.00		0.0	Coarse sand	
1/2 0.50	500	1.0	Medium sand	Sand
1/4 0.25	250	2.0	Fine sand	
1/8 0.125	125	3.0	Very fine sand	
1/16 0.0625	63	4.0	Coarse silt	
1/32 0.031	31	5.0	Medium silt	
1/64 0.0156	15.6	6.0	Fine silt	Silt
1/128 0.0078	7.8	7.0	Very fine silt	
1/256 0.0039	3.9	8.0	Clay	
0.00006	0.06	14.0		Mud

Figure 4. Udden-Wentworth grain-size classification of terrigenous sediments (from Wentworth, 1922).

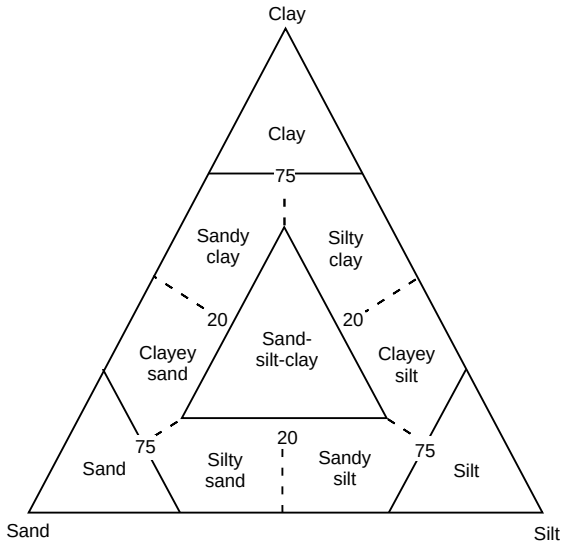

Figure 5. Diagram showing classification scheme used for siliciclastic sediments and rocks during Leg 166 (after Shepard, 1954).

to describe sediments that are composed of calcareous or siliceous pelagic grains of uncertain origin.

The compositional terms for nonpelagic calcareous grains include the following major and minor modifiers as skeletal and nonskeletal grains:

1. *Bioclast* (or *bioclastite*): fragment of skeletal remains (specific names such as molluscan or algal also can be used);
2. *Ooid* (or *oolite*): spherical or elliptical nonskeletal particles smaller than 2 mm in diameter, having a central nucleus surrounded by a rim with concentric or radial fabric;
3. *Pisolite:* spherical or ellipsoidal nonskeletal particle, commonly greater than 2 mm in diameter, with or without a central nucleus but displaying multiple concentric layers of carbonate;
4. *Pellet* (*-al*): fecal particles from deposit-feeding organisms;
5. *Peloid* (*pel*): micritized carbonate particle of unknown origin;
6. *Intraclast:* reworked carbonate sediment/rock fragment or rip-up clast consisting of the same lithology as the host sediment;
7. *Lithoclast:* reworked carbonate-rock fragment consisting of a different lithology than the host sediment;
8. *Calcareous, dolomitic, aragonitic, sideritic:* the mineral composition of carbonate muds or mudstones (micrite) of nonpelagic origin.

The textural designations for siliciclastic grains utilize standard major and minor modifiers such as *gravel*(*-ly*), *sand*(*-y*), *silt*(*-y*), and *clay*(*-ey*). The character of siliciclastic grains can be described further by mineralogy using modifiers such as "quartz," "feldspar," "glauconite," "mica," "lithic," or "calcareous." In addition, the provenance of rock fragments (particularly in gravels, conglomerates, and breccias) can be described using modifiers such as sed-lithic and meta-lithic. The fabric of a sediment can be described using major modifiers such as grain-supported, matrix-supported and imbricated. Generally, fabric terms are useful only when describing gravels, conglomerates, and breccias.

BIOSTRATIGRAPHY

Preliminary ages were assigned primarily based on core-catcher samples. Samples from within the cores were examined when a refined age determination was necessary or when the core-catcher material was barren of calcareous microfossils. Calcareous nannofossils and planktonic foraminifers were examined for biostratigraphic zonation, whereas benthic foraminifers were used to estimate paleobathymetry and to identify periods of downslope transport of platform-derived material.

Ages for nannofossil and planktonic foraminiferal events used during Leg 166 (Fig. 6) are mainly based on the geomagnetic polarity time scale (GPTS) of Berggren et al. (1995a, 1995b). The ages of epoch boundaries were taken from the above-mentioned time scale, except for the Miocene/Pliocene boundary, that we approximated using the nearest biohorizon (top of *Discoaster quinqueramus* [calcareous nannofossil]; 5.6 Ma). Age-depth plots were produced for each site. The depth (mbsf) of a certain datum level was calculated by taking into account the sampling interval. Depth of the biohorizon (i.e., first or last occurrence of a species) was calculated by averaging the depths of the upper and lower limits of the possible range of occurrence. In some cases, two or three holes were used at a site to reduce the range of the depth limits. The age-depth curves were constructed by extrapolation between the best constrained datum levels in terms of depth and age. Preliminary ages were assigned to the seismic sequence boundaries by using the age-depth plots. These ages are tentative only as the tie points were subjectively chosen. Also, the ages await further refinement by reducing the sampling interval.

Calcareous Nannofossils

The zonal scheme established by Martini (1971) was used during Leg 166 for sediments of Cenozoic age. Age estimates for all datums and their relationships to the GPTS in the Miocene to early Pliocene were based on Berggren et al. (1995b). Pliocene to Quaternary biohorizons were modified from Takayama and Sato (1987), Sato et al. (1991), and Sato and Kameo (1996). These additional nannofossil biostratigraphic events that were not in Martini's (1971) zonal framework are shown in Figure 6.

Nannofossil slides were prepared from unprocessed material using standard techniques. Calcareous nannofossil preservation was assessed as

G (good) = little or no evidence of dissolution and/or overgrowth,

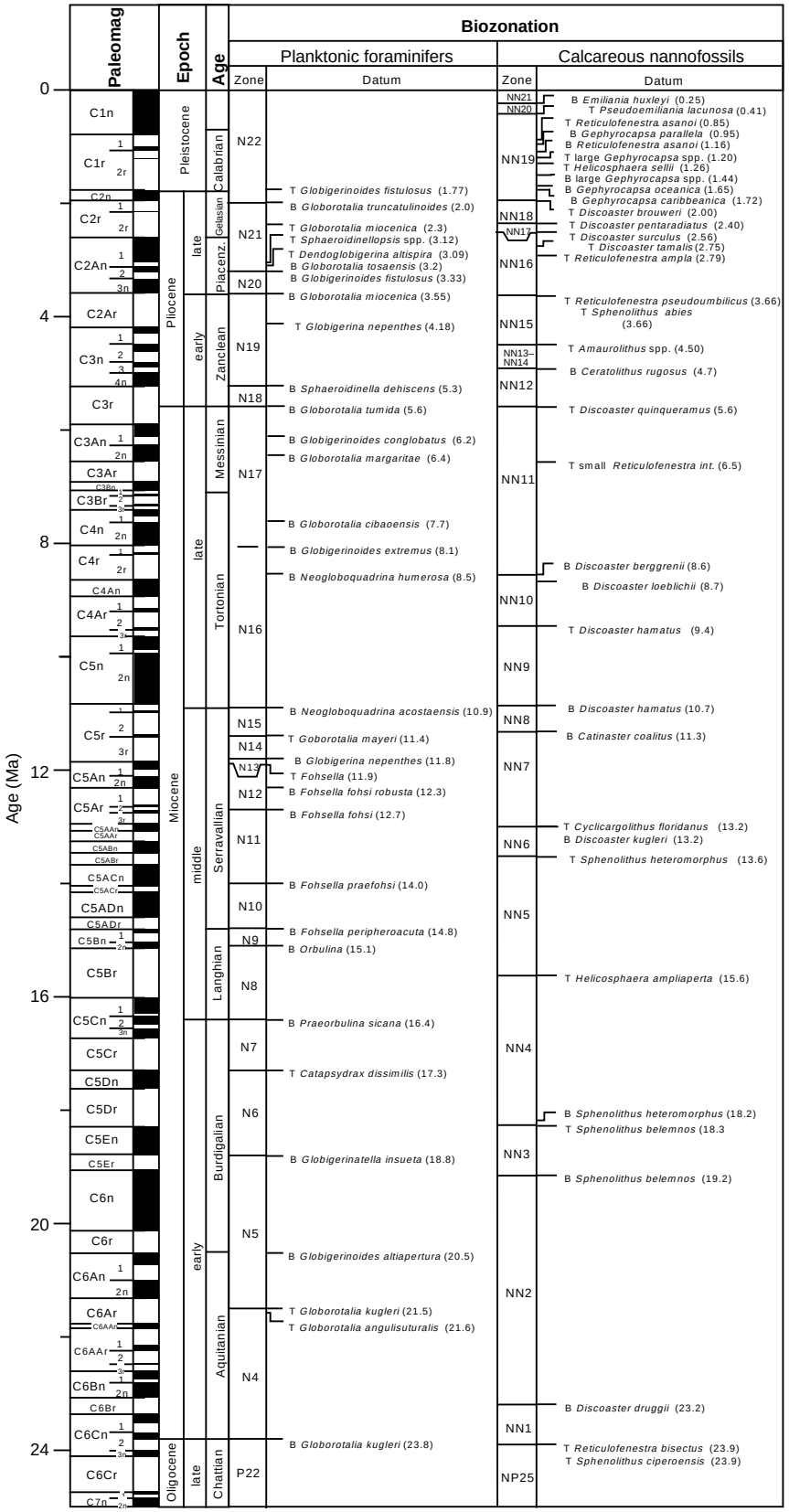

Figure 6. Correlation chart for the interval between 0 and 25 Ma. Nannofossil and planktonic foraminifer zonation and age estimates for important bio-events. The Cenozoic GPTS is from Berggren et al. (1995b).

M (moderate) = minor dissolution or crystal overgrowth observed, and
P (poor) = strong dissolution or crystal overgrowth, many specimens unidentifiable.

The total abundance of calcareous nannofossils for each sample was estimated as

A (very abundant) = over 50 specimens per field of view,
C (common) = 10 to 50 specimens per field of view,
F (few) = 1 to 10 specimens per field of view, and
R (rare) = 1 specimen per 2 or more fields of view.

Nannofossil abundances of individual species were recorded as

A (abundant) = 1–10 specimens per field of view,
C (common) = 1 specimen per 2–10 fields of view, and
R (rare) = 1 specimen per >10 fields of view.

Foraminifers

Samples of approximately 20 cm^3 were soaked in a Calgon solution, sieved (63 µm), and dried under a heat lamp. More indurated sediments required light crushing and agitation in a heated Calgon solution. The abundance of planktonic and benthic foraminifers is defined as the percentage of all material >150 µm, or

B (barren) = 0%,
R (rare) = <10%,
C (common) = 10%–80%, and
A (abundant) = >80%.

Three classes of foraminiferal preservation were designated as

P = poor (almost all specimens were broken),
M = moderate (30%–90% of specimens showed dissolution or breakage), and
G = good (>90% of specimens were well preserved and unbroken).

Planktonic Foraminifers

Bio-events used to assign zonation boundaries and provide age estimates in Leg 166 material are shown in Figure 6. The zonal scheme of Blow (1969), with slight modifications by Kennett and Srinivasan (1983) and Curry et al. (1995), was used here for the Cenozoic. Age estimates for Cenozoic datum levels were taken from Berggren et al. (1995a, 1995b), except for the first occurrence of *Globigerinoides conglobatus* at 6.2 Ma (Chaisson and Pearson, in press). The >150-µm fraction was examined for planktonic foraminifers. The 63- to 150-µm fraction was studied for the zonal markers if they were absent in the larger size fraction.

Benthic Foraminifers

Benthic foraminifers were examined from the >150-µm size fraction. Paleobathymetric estimates were primarily based on van Morkhoven et al. (1986). Bathymetric zones were defined as follows: neritic (0–200 m) was divided into inner (0–30 m), middle (30–100 m), and outer (100–200 m); bathyal was divided into upper (200–600 m), middle (600–1000 m), and lower (1000–2000 m); and abyssal was divided into upper (2000–3000 m) and lower (>3000 m).

The relative abundances of benthic foraminifers were estimated as

B (barren),
R (rare) = <1% of the fauna,
F (few) = 1%–3% of the fauna,
C (common) = 3%–10% of the fauna, and
A (abundant) = >10% of the fauna.

PALEOMAGNETISM

Paleomagnetic studies on the *JOIDES Resolution* during Leg 166 included measurement of magnetic susceptibility on the multisensor track (MST), measurement of natural remanent magnetization (NRM), and measurement of remanence after one or two alternating field (AF) demagnetization steps. The archive half of the core was used for all whole-core measurements in the shipboard magnetometer. The core was subjected to one AF demagnetization step to remove any weak, secondary magnetization. During most of the shipboard measurements, only one AF demagnetization step (10 or 15 mT) was used to determine magnetic polarity. The use of only one demagnetization step was dictated by the relatively rapid rate in which the core was recovered, due partly to the shallow water depth of the sites. Based on results from similar carbonate slope facies cored during the Bahamas Drilling Project (McNeill et al., in press), magnetization in pure carbonate sediments of late Cenozoic age is often dominated by single-domain magnetite. The characteristic (depositional or early postdepositional) remanent magnetization directions were determined, where possible, from NRM and this one-step demagnetization. Confirmation of these directions will be necessary using shore-based discrete sample analysis. Directional data after 10 or 15 mT AF demagnetization from this fine-grained magnetite remanence often still contained an overprint that masked depositional polarity. Where evidence (stability and intensity of remanence, continuity of polarity zones, repeatability of measurements) existed for primary remanence after the AF demagnetization, inclination directions were used to assign a magnetic polarity to the sediment column. With the aid of shipboard biostratigraphic data (planktonic foraminifers and calcareous nannofossils; see Fig. 6), the polarity reversal zones were correlated with the geomagnetic polarity time scale (GPTS) of Cande and Kent (1995). We used the biogeochronology of Berggren et al. (1995b) for the aforementioned biostratigraphic age constraints. Where more than one possible magnetostratigraphic correlation exists due to low-resolution age constraints, both possible correlations are presented and discussed.

In cases where the core was oriented using the Tensor technique, the shipboard directional data were not corrected because we encountered problems with the cryogenic magnetometer data (see below).

Shipboard Instruments

The *JOIDES Resolution* maintained two magnetometers for measuring magnetic remanence during Leg 166: a Molspin spinner magnetometer (replaced at the beginning of Leg 165, December 1995) and a 2G Enterprises (Model 760R) pass-through cryogenic superconducting rock magnetometer (SRM). Measurements were performed on the split-core sections and several discrete samples for characterization of magnetic remanence. Additional discrete samples were collected for subsequent shore-based magnetostratigraphic and rock magnetic studies. The split-core sections were thus used to determine a shipboard magnetostratigraphy. An AF degausser (Model 2G600) capable of alternating fields up to 25 mT was online with the cryogenic magnetometer. Both the SRM and AF coils are encased in a Mu-metal shield, and an automated sample-handling system moves the half-core through the AF coils and magnetometer sense region. SRM measurements were controlled by a modified version of a University of Rhode Island program. During Leg 166 standard orientation conventions were used for the Northern Hemisphere: inclination values were plotted as positive for normal polarity and negative for reversed polarity.

The superconducting quantum interference device (SQUID) sensors in the SRM measure magnetization over an interval approximately 20 cm long. The widths of the sensor region suggest that as

much as 150 cm^3 of core contributes to the output signal. The large volume of core material within the sensor region allows measurement of remanence in weakly magnetized samples, despite the relatively high background noise related to the motion of the ship. Almost all measurements during Leg 166 were performed with the SQUID electronics operating at a 1× scale because of the relatively weak magnetic remanence of carbonate sediments (see cautionary note below).

Saturation experiments conducted aboard ship employed an ASC Scientific Model IM-10 impulse magnetizer to produce an applied field. Magnetization with progressively stronger applied fields, usually to saturation, was measured on either the Molspin spinner magnetometer or the cryogenic magnetometer. Saturation isothermal remanent magnetization (SIRM) acquisition results from representative samples were used to delineate the nature of magnetic remanence in the limestones, nonlimestones, or mixed lithofacies.

Cautionary Note Regarding Cryogenic Magnetometer Data

Paleomagnetic measurements of split core sections, using the whole-core pass-through cryogenic magnetometer, were hindered by low magnetic intensity of the carbonate sediments recovered, axial bias within the magnetometer, and possibly radial remagnetizations. These obstacles manifested themselves in the form of an artificial magnetic direction that possessed a shallow positive inclination and northerly declination. Furthermore, when these split core sections were inverted and rotated within the magnetometer, no change in inclination or declination occurred. Two principal factors are believed to be responsible. First, the split core configuration tends to bias an attenuated low intensity signal in favor of the positive *x*-axis because the core lies in the lower saddle of the "X" SQUID pickup coil. This results in a large value for *x* compared with *y* and *z*, and therefore a shallow positive inclination. Second, the problem appears to have been compounded by the acquisition of a radial remagnetization, which causes the signal in the *y* axis to cancel itself in the split core configuration, thus reinforcing the *x* value. As a result, the *x* value dominates *y* and *z* values, creating a magnetic direction that is an artifact of low magnetic intensity, magnetometer axial bias, and radial remagnetization.

To test the reliability of the measurements and establish criteria that could be used to filter the data, numerous split-core sections were reversed in the cryogenic magnetometer and the *z*:*x* ratio was noted when the sign of the inclination value changed. As shown in Figure 7, a polarity change can typically be observed when the *z*:*x* ratio is higher than 0.7. As a result, provided the *z*:*x* ratio was ≥0.7, the paleomagnetic measurement was regarded as reliable and used to tentatively define a magnetostratigraphy.

Magnetic Susceptibility

Low-field magnetic susceptibility was measured continuously for each unsplit APC core and longer core pieces of XCB samples. Whole-core susceptibility was measured on the MST with a Bartington MS2 susceptibility meter with a MS1/CX 80 whole-core sensor at 0.465 kHz. MST susceptibility measurements were performed at either 5- or 10-cm intervals, usually at the 0.1 scaling. Drift in the susceptibility meter was determined by a measurement at the beginning and end of each run, and a linear correction was applied. Raw susceptibility data were not converted to SI volume ratios. A conversion to SI volume ratios is possible where the core is assumed to be a cylinder with a diameter of 68 mm, and multiplying the raw data by 0.63 × 10^{-5} (Shipboard Scientific Party, 1993).

Core Orientation and Sampling

Leg 166 paleomagnetic measurements for the half-core sections follow the standard ODP core orientation convention (Shipboard Scientific Party, 1991a; Fig. 8). This convention depicts the *z*-axis as being downhole parallel to the core, and the *x*-axis forming a line perpendicular to the split face of the core and directed into the working half, toward a reference mark (a double line) along the center of the core liner on the working half. Discrete sample cubes were marked with an arrow in the negative-*z* (uphole) direction on the plane representing the split surface of the core. The Tensor orientation tool was used during APC drilling for core orientation (see Shipboard Scientific Party, 1994a for a detailed discussion). Data from the Tensor

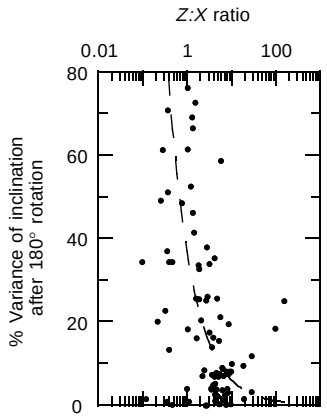

Figure 7. Plot of experimental data showing the *z*:*x* ratio of axial data from the cryogenic magnetometer vs. the percent variance of inclination angle after 180° rotation (i.e., sample run upside down in magnetometer). These data, albeit not a clear delineation, suggest a *z*:*x* ratio of at least 0.7 is needed to produce low variance and provide some degree of measurement reliability. See text for further discussion.

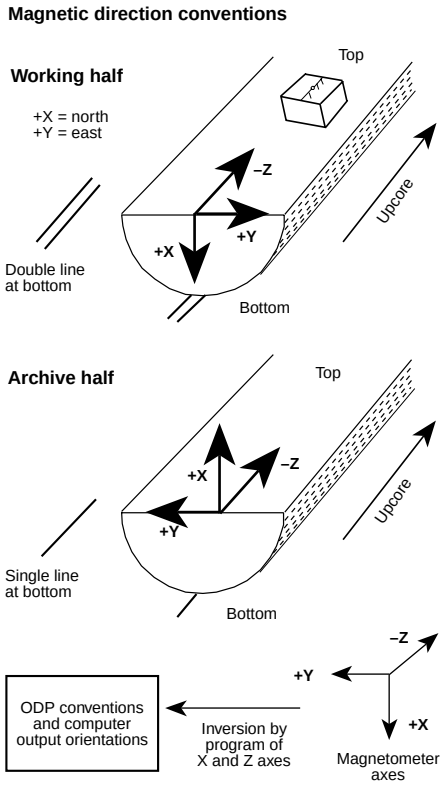

Figure 8. Diagram summarizing the magnetic direction conventions used during Leg 166 for the cryogenic magnetometer.

tool were corrected for local magnetic variation before being used to determine directional data. Tensor orientation data (Table 3) are reported as the angle of the double line reference clockwise from magnetic north. Discrete samples were collected in nonindurated units of the working-half cores by pressing a standard 6-cm^3 plastic cube into the sediment. The plastic cube sampling interval for stratigraphic purposes was 1 sample per section (1.5 m). A higher sampling interval, usually 1 sample per 20 cm was used for shore-based, high-resolution rock magnetic studies. Indurated core was sampled by drilling a 2.5-cm-diameter minicore or by cutting a rectangular block.

COMPOSITE DEPTHS

Composite Section Development

During Leg 166 the continuity of the recovered sedimentary sequence was confirmed by the development of composite depth sections at the multiple-cored sites. Drilling multiple holes with coring intervals offset in depth ensures that intervals missing within a single hole are recovered in an adjacent hole. The composite sections were constructed using the methodology developed during Leg 138 (Hagelberg et al., 1992).

At each site, high-resolution (2- to 10-cm interval) measurements of magnetic susceptibility, gamma-ray attenuation porosity evaluator (GRAPE), wet-bulk density, natural gamma, and *P*-wave velocity were made on whole cores using the multisensor track (MST) soon after the cores equilibrated to room temperature. In addition, measurements of spectral reflectance were made at 10-cm intervals on the split cores. Using magnetic susceptibility and spectral reflectance in the 700-nm band as the primary lithologic parameters, the measurements from each hole were visually and quantitatively compared to determine if coring offsets were maintained between holes. Correlation of events present in multiple holes provided verification of the extent of recovery of the sedimentary sequence. Integration of at least two different physical properties allowed hole-to-hole correlations to be made with greater confidence than would be possible with only a single parameter.

Hole-to-hole correlations were made using an interactive software package that was developed specifically for this task at the Lamont-Doherty Earth Observatory, based on the Leg 138 core-correlation software. Corresponding features in the data from cores in adjacent holes were aligned both graphically and using the computed cross-correlation function. Correlative features were aligned by adjusting the ODP meters below seafloor (mbsf) depths for a given core, on a core-by-core basis. No depths were adjusted within a given core. The results from the multiple lithologic parameters (primarily magnetic susceptibility and GRAPE) were integrated to resolve discrepancies. The resulting adjusted depth scale is the meters composite depth (mcd) scale. For each core at each site, the depth adjustment required to convert from mbsf depth to mcd is given in tabular form in the site chapter.

Figure 9 illustrates the mcd scale and the need for hole-to-hole correlation. In the left panel, magnetic susceptibility records from both holes at Site 1006 are given on the mbsf depth scale. In the right panel, the same records are given after depth-scale adjustment. After adjusting the depth scale so that features common to cores in both holes are aligned, a coring gap is indicated, for example, between Cores 166-1006B-4H and 5H.

The correlation process was iterative. Records of a single physical parameter were moved along a depth scale, core by core, as correlation points between the data at two different holes were picked. Although core distortion within a given core was in some cases significant, the core depths were only adjusted by a single constant for each core. The amount of adjustment necessary to optimize the correlation among multiple holes was retained for each core in each hole. As discussed below, depth adjustments for individual cores were also constrained so that a single spliced record could be sampled from the

Table 3. Summary of Tensor orientation for APC cores.

Date	Hole	Core	Core orientation angle	Hole inclination	Hole azimuth
2/24/96	1003A	3H	314	1.89	334
		4H	77	1.45	357
		5H	104	1.58	8
		6H	357	1.58	6
		7H	131	1.51	9
		8H	339	1.42	2
		9H	226	1.26	9
3/7/96	1004A	3H	233	0.62	60
		4H	112	0.42	35
		5H	91	0.54	58
		6H	12	0.73	49
		7H	137	0.58	60
		8H	5	0.79	77
		9H	17	0.69	199
		10H	359	0.66	58
		11H	266	0.58	46
		12H	217	0.49	55
3/7/96	1005A	4H	159	2.46	161
		5H	271	0.89	120
		6H	162	1.49	168
		7H	12	1.64	141
		8H	161	1.76	75
		9H	209	1.16	118
3/15–16/96	1006A	3H	30	0.81	67
		4H	259	1.16	68
		5H	151	1.14	64
		6H	165	1.18	67
		7H	198	1.13	66
		8H	232	1.06	70
		9H	264	0.91	75
		10H	349	0.73	78
		11H	246	0.83	74
		12H	250	0.84	69
		13H	266	0.78	64
	1006A	14H	296	0.71	50
		15H	5	0.82	47
		16H	147	0.67	53
		17H	216	0.64	51
		18H	14	0.70	52
		19H	207	0.60	60
		20H	265	0.63	49
		21H	244	0.62	46
		22H	320	0.73	42
		23H	119	0.74	46
		24H	41	0.98	46
		25H	206	0.93	37
		26H	316	1.16	45
		27H	227	1.18	33
	1006A	28H	254	1.30	34
		29H	53	1.25	35
3/19/96	1006B	3H	277	2.17	299
		4H	53	1.62	28
		5H	88	1.68	27
		6H	91	1.85	36
		7H	26	1.91	38
		8H	88	1.83	42
		9H	258	1.69	37
		10H	194	1.64	38
		11H	237	1.62	34
		12H	116	1.59	38
		13H	46	1.66	38
		14H	162	1.42	39
		15H	32	1.38	39
		16H	196	1.15	39
		17H	168	1.03	37
		18H	195	1.00	35
		19H	321	1.10	27
3/19/96	1006C	1H	333	1.44	148
3/19/96	1006D	1H	91	1.34	173
3/24/96	1007B	3H	187	1.13	243
		4H	217	0.67	275
		5H	—	—	—
		5H	107	0.85	246
		6H	*	*	*
		7H	19	1.18	210
		8H	11	1.14	239
		9H	265	0.68	224
		10H	254	0.82	280

Note: — = no shot, * = data suspect.

aligned cores without any additional depth scale changes. The same process was then repeated for the other lithologic parameters to check the core adjustments. Where the amount of offset necessary to align features was ambiguous or uncertain for both lithologic parameters, or where multiple hole data were unavailable, no depth adjustment for that particular core was made. In these cases, the total amount of offset between mbsf depth and mcd is equal to the cumulative offsets from the overlying cores. When complete, the composite depth section was compared with biostratigraphic and lithologic observations of distinctive markers such as carbonate hardgrounds from multiple holes, for quality control.

The composite depth section for each site is presented in tabular format. A portion of the composite depth table for Site 1006 is provided as an example in Table 4. For each core, the last two columns in Table 4 give the depth offset applied to the mbsf depth, respectively. The offset column facilitates conversion of samples that are recorded in mbsf depths to composite section depth. By adding the amount of offset to the sub-bottom depth (mbsf depth) of a measurement taken in a particular core, the equivalent in mcd is obtained. Thus, the depth conversion table can serve as a guide for future sampling.

After composite depth construction, a single spliced record that was representative of the multiple-cored sedimentary sequence was assembled. The missing intervals of the sedimentary sequence from a single hole could be identified, and so missing intervals were patched in with data from adjacent holes. By identifying the intervals where features present in the multiple holes were most highly correlated, it was possible to construct a spliced record without the danger of mistakenly duplicating any individual features or cycles. Because there is considerable stretching and/or compression of many sections of core relative to the same core in adjacent holes, the precise length of the spliced record depends on which intervals of core are selected to build it. In particular, APC core tops were generally expanded relative to equivalent intervals located within the middle of the core in adjacent holes, and the bases of cores were relatively compressed. To prevent the composite section from having a different set of depth offsets than the splice, the composite section was constructed so that cores were placed in exact alignment with splice tie points. In general, this alignment is slightly different than the alignment that gives the highest hole-to-hole correlation, and thus sometimes gives the visual impression that core alignment is not perfect. Further adjustments to the composite depth section on a within-core basis are required to align all features exactly.

An example of a spliced magnetic susceptibility record from Site 1006 is given in Figure 10. The spliced magnetic susceptibility record is plotted to the right of the aligned Hole 1006A and 1006B data used to construct the splice. Splices were made at the same mcd level from core to core, assuring that mcd and spliced section depths are identical. Tables listing the tie points for construction of the spliced record are included in each site chapter; an example is presented in Table 5. A significant advantage of the spliced record is that it provides a single representative record of a lithologic parameter (i.e., susceptibility, color reflectance, or natural gamma) for a given site. This single record is ideally suited to serving as a sampling scheme for high-resolution paleoceanographic studies.

ORGANIC GEOCHEMISTRY

Shipboard organic geochemistry during Leg 166 included the following analysis: (1) determination of total carbonate carbon in whole rock; (2) elemental analyses of carbon, nitrogen, hydrogen, and sulfur in whole rock and acid residues from carbonates; (3) determination of free hydrocarbons, petroleum potential, and thermal maturity of organic matter; and (4) analyses of hydrocarbon gases. Detailed procedures are described by Emeis and Kvenvolden (1986) and in Shipboard Scientific Party (1995b).

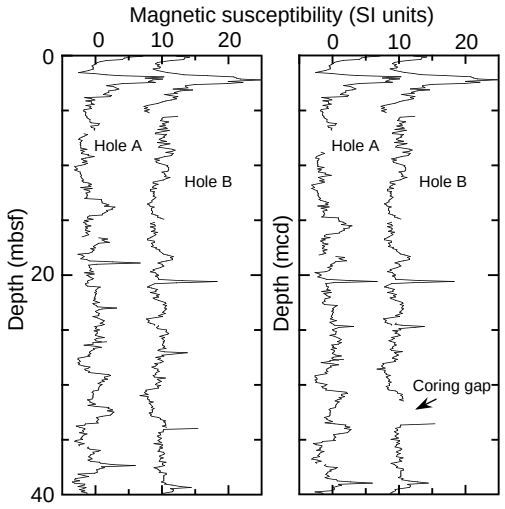

Figure 9. Portions of the magnetic susceptibility records from Site 1006. Left: Cores 166-1006A-1H through 4H, and 166-1006B-1H through 5H on the mbsf depth scale. Data from each hole are offset for clarity. Right: The same cores on the mcd depth scale. The composite depth section has the advantage that features common to all holes are in relative alignment. Arrow refers to coring gap mentioned in text.

Table 4. Partial composite depth table from Site 1006.

	1006A		1006B	
Core	Depth (mbsf)	Offset	Depth (mbsf)	Offset
1	0	0	0	0
2	7.1	1.7	5.5	0
3	16.6	1.7	15	0
4	26.1	1.61	24.5	–2.4
5	35.6	1.61	34	–0.39
6	45.1	2.81	43.5	2.41
7	54.6	2.81	53	2.81
8	64.1	2.81	62.5	2.41

Note: Add the offset to the depth (mbsf) to determine the mcd.

Inorganic Carbon

Carbonate carbon concentrations were determined using a Coulometrics NA5011 carbon-dioxide coulometer. Sediments were generally analyzed at a frequency of three samples per core. A sample of approximately 10 mg of freeze-dried, ground sediment was reacted with 3N HCl. The liberated CO_2 was back-titrated to a coulometric endpoint. Calibration was performed using pure calcium carbonate as a standard. Percentage of carbonate is calculated from the inorganic carbon (IC) content with the assumption that all inorganic carbon is present as calcium carbonate:

$$CaCO_3 = IC \times 8.332.$$

No corrections were made for the presence of either siderite or dolomite (Shipboard Scientific Party, 1991c). The precision of the IC measurements is 2%.

Elemental Analyses

Total carbon, nitrogen, and sulfur were determined using a Carlo Erba 1500 NCS Analyzer. Sediments were generally analyzed at a frequency of one sample per one or two cores. Approximately 5 mg of freeze-dried, ground sediment was combusted at 1000°C in a stream of oxygen. Using He as a carrier gas, the oxygen was removed

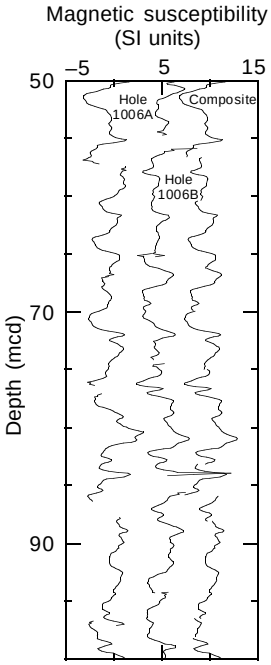

Figure 10. A portion of the aligned magnetic susceptibility record from Site 1006. Spliced composite core data from the multiple holes are plotted on the right. Data are plotted on the mcd scale. For clarity, Hole 1006B data are offset by five units and the composite data by 10 units.

Table 5. Partial splice table from Site 1006.

Hole	Core	Depth (mbsf)	Depth (mcd)		Hole	Core	Depth (mbsf)	Depth (mcd)
A	1H	6.15	6.15	tie to	B	2H	6.15	6.15
B	2H	14.45	14.45	tie to	A	2H	12.75	14.45
A	2H	15.45	17.15	tie to	B	3H	17.15	17.15
B	3H	23.25	23.25	tie to	A	3H	21.55	23.25
A	3H	22.95	24.65	tie to	B	3H	24.65	24.65
B	3H	32.85	30.45	tie to	A	4H	28.85	30.45
A	4H	35.25	36.86	tie to	B	5H	37.25	36.86
B	5H	42.39	42.00	tie to	A	5H	40.4	42.00

and the combustion products were reduced. The reduced gases were separated by gas chromatography and quantified with a thermal conductivity detector (TCD) (Emeis and Kvenvolden, 1986). Sulfanilamide was used as the primary standard, and the National Institute of Standards and Technology's (NIST) Eustarine Sediment as the secondary standard. The precision for the three elements was 1.1% for total nitrogen (TN) at 0.15 wt% N, 0.7% for total carbon (TC) at 2 wt% C, and 2% for total sulfur (TS) at 1 wt% S. The total organic carbon (TOC) was calculated as the difference between TC and inorganic carbon (IC):

$$\text{TOC (wt\%)} = \text{TC (wt\%)} - \text{IC (wt\%)}.$$

The precision of the TOC determinations is defined by the combined precision of the TC and IC methods and is generally not better than 2%.

Organic Matter Characterization and Maturation

The type of organic matter in a selected group of samples was characterized by pyrolysis using a Delsi Nermag Rock-Eval II system. This method is based on a whole-rock pyrolysis technique designed to identify the type and maturity of organic matter and to detect the petroleum potential of the sediments (Tissot and Welte, 1984; Espitalié et al., 1986). The Rock-Eval system includes a temperature program that first releases volatile hydrocarbons (S_1) at 300°C for 3 min. Hydrocarbons are then released via thermal cracking of kerogen (S_2) as the temperature is increased from 300°C to 550°C at 25°C/min. S_1 and S_2 hydrocarbons are measured by a flame ionization detector (FID) and reported in milligrams per gram of sediment. The temperature at which the kerogen yields the maximum amount of hydrocarbon during the S_2 program provides T_{max}, a parameter used to assess the maturity of the organic matter. Between 300°C and 390°C of the stepped pyrolysis, CO_2 released from the thermal degradation of organic matter (S_3) is trapped and measured by a TCD in milligrams per gram of sediment. Rock-Eval II parameters help in characterizing organic matter by allowing the following indices to be calculated: Hydrogen Index (HI; $S_2/TOC \times 100$), Oxygen Index (OI; $S_3/TOC \times 100$), S_2/S_3 ratio, and Productivity Index (PI; $S_1/(S_1+S_2)$. Interpretation of Rock-Eval data is considered to be compromised for samples containing less than 0.5% TOC (Peters, 1986).

Hydrocarbon Gases

For safety reasons, concentrations of the light hydrocarbon gases C_1 through C_3 (methane, ethane, and propane) were monitored in each core or whenever gas pockets were encountered. Gases were extracted using the headspace technique for bulk sediments, described by Kvenvolden and McDonald (1986), or by using a vacutainer for sampling gas pockets directly though the core liner. Headspace analyses were performed on 5-cm^3 sediment samples heated in sealed vials at 60°C for 30 min before gas analysis. Immediately after retrieval and cutting of the core, a No. 6 cork borer with a calibrated plunger was used to obtain a measurable volume of sediment from the core.

Headspace and vacutainer gas were both routinely analyzed using a Hewlett Packard 5890 II plus gas chromatograph (GC) equipped with a 2.4 m × 0.32 cm stainless steel column, packed with HaySep S (80–100 mesh), and a FID detector. This instrument measures concentrations of methane, ethane, ethylene, propane, and propylene. Either the vacutainer or the headspace syringe was directly connected to the gas chromatograph via a 1.0-cm^3 sample loop. A Hewlett-Packard 3365 Chemstation was used for data collection and evaluation. Calibration was made by using Scotty IV analyzed gases.

When the presence of higher concentrations of C_{2+} hydrocarbons was suspected, gas samples (collected as described before) were injected into the Natural Gas Analyzer (NGA), which measures hydrocarbons from methane to hexane. The NGA consists of a Hewlett-Packard 5890 II, plus GC, equipped with a 60 m × 0.32 mm DB-1 capillary column and a FID detector. Nonhydrocarbon gases could be analyzed at the same time via a packed column and a TCD detector. For hydrocarbon analysis the GC oven was heated from 80°C to 100°C at 8°C/min and then to 200°C at 30°C/min.

The background concentration of methane was regularly monitored in the laboratory and on the core deck. Average values were between 2 and 3 ppm. The precision of both gas analyses was approximately 5%.

INORGANIC GEOCHEMISTRY

Interstitial Water Sampling and Chemistry

The inorganic geochemistry program initiated during Leg 166 was designed to provide rapid results to aid in shipboard sampling and identification of key lithologic sections. The bulk of the shipboard inorganic geochemistry centered around the analyses of squeezed interstitial waters, and on quantifying mineralogy of the solid carbonate samples.

Shipboard interstitial water analyses were performed on 5- to 15-cm-long whole-round sections that were cut immediately after core

retrieval on deck. Details of the sampling resolution are described in the individual site chapters (this volume). After extrusion from the core liner, the surface of each whole-round section was carefully scraped with a spatula to remove potential contamination. Interstitial waters were collected using a titanium squeezer, modified after the standard ODP stainless steel squeezer of Manheim and Sayles (1974). After the squeezer was loaded, pressure up to 40,000 lb (approximately 4150 psi) was applied using a hydraulic press, and pore water was extruded through prewashed Whatman No. 1 filters fitted above a titanium screen.

All interstitial water samples were double-filtered. Interstitial water was collected into acid-washed (10% HCl) 50-mL plastic syringes through 0.45 µm Gelman polysulfone disposable filters. The interstitial water was subsequently re-filtered through either 0.45 µm Gelman polysulfone disposable filters or acid-washed 0.22 µm Gelman polysulfone disposable filters in the case of samples for shore-based trace element analyses. Samples for shipboard work were stored in plastic vials prior to analysis.

In the deeper portions of the core (below 200 m), interstitial water sampling became more difficult due to the high degree of lithification found in the sediments. In such cases, whole-round or half-round samples were selected from the softest portions of the core, placed inside several plastic bags, and crushed with a hammer. The crushed sample was then squeezed in the normal manner described above.

Interstitial water samples were routinely analyzed for salinity as total dissolved solids with a Goldberg optical handheld refractometer. The alkalinity was measured by Gran titration with a Brinkmann pH electrode and a Metrohm autotitrator. The pH was measured and calibrated using NBS buffers as part of the alkalinity titration. In situ electrode potential measurements were made prior to squeezing in the whole-round using a glass combination electrode and an Orion portable pH meter. The electrode was calibrated against TRIS and BIS buffers to calculate pH on the free H^+ scale. When samples contained a substantial concentration of CO_2, the pH (herein referred to as pmH) determined in situ was more reliable than that obtained during the alkalinity titration. This occurs because the algorithm employed for pH measurement before the start of the alkalinity titration was adversely affected by degassing.

Dissolved Cl^- was determined by titration. Because high concentrations of HS^- interfere with the Cl^- titration by causing the precipitation of Ag_2S, sample aliquots taken from highly anoxic samples were pre-oxidized by adding 100 µL 30% H_2O_2 to the sample approximately 5 min before the titration.

Silica (H_4SiO_4), phosphate (HPO_4^{2-}), and ammonium (NH_4^+) were determined by spectrophotometric methods with a Milton Roy Spectronic 301 spectrophotometer (Gieskes et al., 1991). A modification of the standard analytical methods involved removing sulfide from samples analyzed for HPO_4^{2-} and H_4SiO_4 by acidifying with 20 µL concentrated HCl and purging with nitrogen for 10–15 min. This procedure was implemented because at Site 1003, it was found that the presence of large amounts of hydrogen sulfide interfered with the HPO_4^{2-} and H_4SiO_4 analyses. Subsequent checks on the treated sample with mercuric chloride indicated that most of the sulfide had been successfully removed. Additional samples were fixed for shore-based analysis of sulfide using a solution of 10% zinc acetate. The standard deviations of analyses were alkalinity, <1.5%; Cl^-, <0.4%; and H_4SiO_4, HPO_4^{2-}, and NH_4^+, ~5%.

Sodium (Na^+), potassium (K^+), magnesium (Mg^{2+}), calcium (Ca^{2+}), and Cl^- and sulfate (SO_4^{2-}) were analyzed by ion chromatography using a Dionex DX-100. The 1 sigma standard deviations were K^+, <6%; Mg^{2+} and Ca^{2+}, <2%; SO_4^{2-}, <4%; and Na^+, <5%. Chloride measurements by ion chromatography were systematically higher by approximately 3%–5% compared to those obtained by titration; hence, titration results are reported. The concentration of dissolved Ca^{2+} and Mg^{2+} in selected samples collected from the first site was also determined by titration with EGTA and EDTA, and the results compared to the ion chromatography results. No systematic difference was noted, and all subsequent analyses were performed by ion chromatography.

Iron (Fe^{2+}), lithium (Li^+), and strontium (Sr^{2+}) concentrations were quantified using flame atomic emission (AES) or absorption (AAS) spectrometry on a Varian AA-20. Iron was determined directly in the alkalinity titration residues. As a result of a combination of low concentrations, large matrix effects owing to highly variable sample salinities, and potential contamination during sample handling and alkalinity titrations, the iron data are subject to substantial errors and should only be considered indicative of trends. Fiftyfold dilutions were used for Li^+, and five- to twentyfold dilutions were employed for Sr^{2+} analyses. Air-acetylene (Fe^{2+}, Li^+) and nitrous oxide acetylene (Sr^{2+}) flames were used. Standards for all flame AAS/AES techniques were matched in matrix composition to the samples (Li^+, Sr^{2+}) or prepared in synthetic seawater (Fe^{2+}). A more detailed description of all methods and standards used can be found in ODP Technical Note 15 (Gieskes et al., 1991). The 1 sigma standard deviations were better than 2% for Li^+, and better than 3%–4% for Sr^{2+}.

Fluoride (F^-) was determined on pore-water samples using an ion-specific combination electrode (Orion Model #96-09) after the method of Froelich et al. (1983). In this method, 0.5 mL of sample was mixed with 0.5 mL of total ionic strength adjustment buffer (TISAB IV, Orion) and allowed to equilibrate and decomplex for 1/2 hr before reading on an Orion pH/mV meter. Calibration was achieved using IAPSO solutions spiked with a fluoride standard and was rechecked periodically during the leg. Ten replicates of surface seawater collected from Site 1004 gave a precision of 3%. During Leg 114, only a minimal influence of temperature and squeezing artifacts was observed on fluoride determination (Shipboard Scientific Party, 1988); thus, no effort was made to correct for these possible influences.

X-ray Diffraction

Mineralogy was determined on solid carbonate samples using X-ray diffraction (XRD). Quantitative XRD analyses were performed on bulk samples to determine the relative percentage of aragonite, calcite, quartz, and dolomite. Samples were run in batches of 36, and scanned from 25° to 35° 2θ at 1°/min. To overcome the limitations of using multicomponent standards, conversion from peak areas to mineral weight percent was accomplished using the H-factor method of Hooton and Giorgetta (1977), modified to use low magnesium calcite (LMC) as the common internal standard. In this method, the areas of the peaks of interest were obtained relative to the calcite peak, and calibrated using calibration curves from a series of two-component standards. The final weight percent of each mineral was adjusted to the appropriate carbonate concentration measured on the same sample (see "Organic Geochemistry" section, this chapter). In addition, the carbonate percentages were corrected for the presence of dolomite after the method described for Leg 133 (Shipboard Scientific Party, 1991b). Overall, the accuracy of the XRD analysis is within 5% actual weight percent, with a standard deviation of 3%.

XRF Analysis

At Sites 1003 and 1005, major and trace element sediment chemistry were determined by X-ray fluorescence (XRF) analysis to aid in the interpretation of data acquired by the geochemical logging tool. Below we briefly summarize the methods used; for a more detailed description of the methodology, including calibrations, see the "Explanatory Notes" chapter in the Leg 165 *Initial Reports* volume (Shipboard Scientific Party, 1997).

Sediment samples were freeze-dried for 24 hr, and then powdered and homogenized by hand with an agate mortar and pestle. Approximately 6 g of unfired sediment sample powder was mixed with 30 drops of Chemplex liquid polymer binder and pressed into an aluminum Spex-cap at 7 tons of pressure using a hydraulic press.

Lithified samples were ground on a diamond-grit grinding wheel to remove saw marks and any outside surfaces exposed to the coring bit. Samples were sonicated once in methanol and then twice in distilled water and dried in a 110°C oven for at least 12 hr. Cleaned rock chips were reduced to a fine gravel (≤5 mm pieces) by crushing the chips between two pieces of Delrin plastic in a hydraulic press, and ground to a powder (≤200 mesh) in a WC-Shatterbox.

Major and trace element abundances were determined using an automated ARL 8420 wavelength-dispersive spectrograph, equipped with an end-window, Rh-target X-ray tube, under measuring conditions outlined in Shipboard Scientific Party (1997). Sediment trace element analyses (Nb, Zr, Y, Sr, Rb, Zn, Cu, Ni, Cr, V, and Ba) were performed on the pressed pellets and corrected for nonlinear background, spectral interferences, and matrix absorption effects using the ARL software package and a range of geologic standards. A smaller suite of major elements (Fe, Mn, Ti, P, and Ca) was measured separately on the same pressed pellet used for the trace element analysis. The spectrometer was calibrated using a suite of well-analyzed reference standards (Shipboard Scientific Party, 1997). Both precision and accuracy were assessed by multiple analyses of Standard Reference Material 1C, an argillaceous limestone from the National Institute of Standards and Technology, Washington, D.C., U.S.A. (Shipboard Scientific Party, 1997).

PHYSICAL PROPERTIES

Introduction

Standard shipboard whole-core measurements of physical properties included nondestructive, multisensor track (MST) measurements of density, *P*-wave velocity, natural gamma ray (NGR), and magnetic susceptibility. Discrete measurements included bulk density, porosity, water content, grain density, thermal conductivity, undrained shear strength, and compressional-wave velocity (V_p). Unless otherwise mentioned, measurements of physical properties were made on whole cores utilizing the MST and on discrete samples from split cores. Thermal conductivity was measured only on unconsolidated whole-round cores. The vertical spacing of the MST measurements was in general maintained at 15 cm for the NGR, and 5 cm for velocity, gamma-ray attenuation porosity evaluator (GRAPE) density, and magnetic susceptibility. The NGR sensor was switched off in sediments with a gamma-ray emission below the background level of 6 cps. In indurated sediments, the *P*-wave logger (PWL) on the MST was switched off. The frequency of the discrete velocity measurements in the unconsolidated intervals was two or three per section with one sample per section taken for index properties. In the semilithified to lithified sediment, the frequency of the velocity measurements was increased to approximately five observations.

Shipboard Measurements

Index Properties

Index properties (bulk density, grain density, water content, porosity, and dry density) were calculated from measurements of wet and dry weights and wet and dry volumes from samples of approximately 15 cm^3. Sample mass was determined aboard ship to a precision of ±0.01 g using a Scitech electronic balance. Volumes were determined using a helium Quantachrome Penta-Pycnometer with an approximate precision of ±0.02 cm^3.

The determination of water content followed the methods of the American Society for Testing and Materials (ASTM) designation (D) 2216 (ASTM, 1989). As outlined in ASTM D2216, corrections are required for salt when measuring marine samples. The recommended equation for the water content calculation, which is the ratio of the pore fluid mass to the dry sediment mass (% dry wt), is as follows.

$$W_c\ (\%\ \text{dry wt}) = (M_t - M_d)/(M_d - rM_t), \quad (1)$$

where W_c is water content reported as a decimal ratio of % dry weight, M_t is total (saturated) mass, M_d is dry mass, and r is salinity.

Bulk density (ρ) is the density of the total sample including the pore fluid. The mass (M_t) was measured using the electronic balance, and the total volume was measured with the helium pycnometer. In high-porosity sediment, the bulk density was calculated using

$$\rho = M_t/V_t, \quad (2)$$

where V_t is the total sample volume.

The porosity (ϕ) was calculated using the equation

$$\phi = (W_c\rho)/([1 + W_c]\rho_w), \quad (3)$$

where W_c is water content reported as a decimal ratio of % dry wt, ρ is bulk density, and ρ_w is the density of the pore fluid.

The grain density (ρ_{grain}) was calculated from the dry mass (Scitech balance) and dry volume (pycnometer) measurements. Both mass and volume were corrected for salt as follows.

$$\rho_{grain} = (M_d - s)/(V_d - [s/\rho_{salt}]), \quad (4)$$

where M_d is the dry mass, s is salt correction, V_d is dry volume, and ρ_{salt} is the density of salt (2.257 g/cm^3).

Dry density (ρ_d) is the ratio of the dry mass (M_d) to the total volume. This value is used for calculations of mass accumulation. The dry density was calculated for the corrected water content (Eq. 1) and porosity for each measurement using the equation

$$\rho_d = (\phi/W_c)\rho_w. \quad (5)$$

Multisensor Track (MST)

The MST includes a gamma-ray attenuation porosity evaluator (GRAPE), a *P*-wave logger (PWL), a natural gamma-ray sensor, and a magnetic susceptibility sensor. Whole-round sections designated for shipboard geochemical analysis were removed prior to scanning. Thermal homogeneity for the remaining core was ensured by allowing time for the cores to equilibrate approximately to room temperature for about 3 hr prior to MST measurements.

The GRAPE measures bulk density and is based on the attenuation of a collimated beam of gamma rays passing through a known volume of sediment (Boyce, 1976). During Leg 166, the measuring interval was usually set at 5 cm. The GRAPE data are most reliable in advanced hydraulic piston corer (APC) and nonbiscuited extended core barrel (XCB) and rotary core barrel (RCB) cores. In biscuited sections, the GRAPE is not used for analyses.

The *P*-wave logger (PWL) on the MST transmits a 500-kHz compressional-wave pulse through the core at a repetition rate of 1 kHz. During Leg 166, measurements were taken usually at 5-cm intervals. Only the APC and nonbiscuited XCB and RCB cores were measured. Weak returns, caused by trapped air between core and liner, with signal strengths below a threshold value were removed.

Magnetic susceptibility was measured on all sections at 10-cm intervals with a sampling period of 10 s. The long sampling period ensured acceptable readings for the usually low susceptibility of carbonates.

The natural gamma intensity device was set to measure at 15-cm intervals with sampling periods of 20 s. Where pipe remained in the hole while logging, the data were used to complete the gamma-ray wire-line log. In the open hole section, they were used to calibrate the wire-line log with the core.

During Leg 166, GRAPE density measurements in unconsolidated lithologies, usually made in the upper 100 to 200 m of sediment, were overall significantly higher (up to 15%) than discrete density measurements, with values of 1.8 to 2.1 g/cm^3 vs. 1.6 to 1.9 g/cm^3,

respectively. In addition, in low-porosity sediments, the GRAPE density was usually lower (up to 5%) than the discrete density measurements. Three explanations are suggested: (1) the MST software does not include a correction for the attenuation effect of high-porosity sediments (Boyce, 1976; Lloyd and Moran, 1992); (2) air, trapped in the sediment-filled beakers (unconsolidated sediments), reduces the relative saturated weight and increases the relative volume measured in the pycnometer, thereby decreasing the resulting bulk density; and/or (3) low-porosity sediments that are semilithified to lithified, have a smaller core diameter, and subsequently, a relatively smaller attenuating volume than the calibrated volume, which results in a lower calculated density. To solve the first problem, GRAPE densities were corrected using the Boyce (1976) equation

$$\rho = [(\rho_{bc} - \rho_{fc})(\rho_g - \rho_f)]/(\rho_{gc} - \rho_{fc}) + \rho_f, \quad (6)$$

where ρ is corrected density, ρ_{bc} is GRAPE density, ρ_{fc} = fluid density calculated from gamma counts (1.128 g/cm^3), ρ_g is true grain density of quartz (2.65 g/cm^3), ρ_f = true fluid density (1.024 g/cm^3), and ρ_{gc} = grain density calculated from gamma counts (2.65 g/cm^3). It is not yet clear how to improve the accuracy of the index property procedure. Therefore, it is assumed that the discrete measurements are more accurate, whereas the GRAPE density gives a reliable high-resolution relative density trend.

Thermal Conductivity

The needle probe technique was used to measure thermal conductivities of soft sediment samples. The "needle probe" is a thin (18 AWG), ~7-cm-long metal tube that contains a thermistor and a heater wire. When inserted into the unsplit core, the probe applies a calibrated heat to the surrounding sediments. The thermal conductivity was determined from the pattern of the temperature rise in response to this heat (Von Herzen and Maxwell, 1959). The needle is assumed to be a nearly perfect conductor because it is much more conductive than unconsolidated sediments. The temperature of the superconductive probe has a linear relationship with the natural logarithm of the time after the initiation of the heat:

$$T(t) = (q/4\pi k) \cdot \ln(t) + C, \quad (7)$$

where T is the temperature, q is the heat input per unit length per unit time, k is the thermal conductivity, t is the time after the initiation of the heat, and C is a constant. All thermal conductivity data are reported in units of watts per meter degrees Kelvin (W/[m·K]). After measuring, the temperature values were plotted against the natural log of the time, and a linear least-squares fit was applied. Conductivity was then calculated from the slope of the linear fit.

Sediment cores were allowed to equilibrate to room temperature prior to these measurements, as an unstable internal temperature of the core may cause large errors in the conductivity determination. Temperature drift of the samples was monitored for 3 min before firing the heater. The duration of the actual measurement was 4 min. The thermistor temperature was read with a ~10-s interval.

During Leg 166, one measurement per core section (i.e., 1.5-m interval) was made. The Thermocon-85 data acquisition unit is capable of operating five needle probes simultaneously. Usually, two core sections were handled at a time. An additional needle could be used to measure the thermal conductivity of a reference sample. These needle probes were calibrated with standard samples: two types of rubber bricks (0.54 W/[m·K] and 0.96 W/[m·K]) and a macor cylinder (1.46 W/[m·K]) as such standards. Their thermal conductivities were determined accurately by the divided bar instrument (Shipboard Scientific Party, 1992).

Routine data reduction also was performed by the Thermocon unit. It produces the temperature vs. time cross plot (in natural log), applies the linear fit, and calculates the standard error of the fit for each measurement. During Leg 166, only the temperature records during the last 2 min of the heater operation were used. The record from the first 2 min was discarded.

The conventional needle probe technique is not suited for measurements of semilithified or fully lithified samples. For lithified samples, a needle probe was attached on a flat surface of a thermally insulating compound. This sensor unit was applied onto the surface of a split core sample. Then, just as for the conventional needle technique, the probe was heated and the subsequent temperature rise was monitored. The theory behind this "half-space" technique has been explained by Vacquier (1985). The reduction of the data is similar to that of the conventional needle technique.

Undrained Shear Strength

The undrained shear strength of the sediment was measured at intervals of two measurements per section using a Wykeham-Farrance motorized vane shear apparatus following the procedures by Boyce (1977). The vane rotation rate was set to 90° per minute and the vane used for all measurements had a 1:1 blade ratio with a dimension of 1.28 cm.

The instrument measures the torque and strain at the vane shaft using a torque transducer and potentiometer, respectively. Output for torque and strain were recorded on a Hewlett-Packard X-Y recorder in volts. The shear strength reported was the peak strength determined from the torque vs. strain plot. In addition to the peak shear strength, the residual strength was determined from the same plot where the failure was not dominated by cracking of the sample.

In the interpretation of shear vane measurements, it is assumed that a cylinder of sediment is uniformly sheared around the axis of the vane in an undrained condition, with cohesion as the principal contributor to shear strength. Departures from this assumption include progressive cracking within and outside of the failing specimen, uplift of the failing core cylinder, drainage of local pore pressures, and stick-slip behavior.

Sonic Velocity

The choice of method for compressional-wave velocity measurements (V_p) was dependent on the degree of consolidation of the sediments.

1. *Unconsolidated sediments*. In unconsolidated sediments, V_p was measured using two pairs of perpendicular oriented Digital Sound Velocimeters (DSV). One pair was aligned vertical to bedding and the other one horizontally, so that sediment anisotropy could be determined. The transducer pairs had a fixed spacing of 7 cm (vertical) and 3.5 cm (horizontal) and were inserted into the split cores of soft sediment. An acoustic signal of 500 kHz was emitted and received by the two transducers. The signal was then digitized by an oscilloscope, and the waveform was transferred to a computer. The first arrival was manually picked and velocity automatically calculated. Anisotropy was then calculated by the difference between the horizontal and vertical velocity using the following equation.

$$\text{anisotropy} = 2(V_{pt} - V_{pl})/(V_{pt} + V_{pl}), \quad (8)$$

where V_{pt} is the transverse compressional-wave velocity and V_{pl}, the longitudinal velocity. The velocity meter was calibrated by measuring V_p in water.

2. *Consolidated samples*. V_p of consolidated zones in the core were measured through the entire split core with a piezoelectric transducer pair with a center frequency of 500 kHz, which is recorded, digitized, and transferred to a computer similar to the one used for unconsolidated samples. For this purpose, the split core was placed between the transducers. The upper transducer was pressed against the

split surface while the lower transducer was pressed against the core liner. Thus, V_p measured through the split cores represent horizontal velocities. Because the measured wave propagation includes the path through the liner, these measurements were corrected for the additional traveltime of passing through the liner. Zero travel times for the velocity transducers were measured with a series of aluminum standards of known length. The axial pressure that was applied between sample and transducer was monitored by a pressure gauge. To improve the coupling between transducer and core, water was applied to the transducer heads.

DOWNHOLE LOGGING

Well-Logging Operations

The Lamont-Doherty Earth Observatory Borehole Research Group (LDEO-BRG) in conjunction with the University of Leicester (Leicester University Borehole Research), the Institute Méditerranéen de Technologie (IMT), and Schlumberger Well-Logging Services, provided the downhole well logging aboard the *JOIDES Resolution* during Leg 166.

After coring was completed, viscous drilling fluid (sepiolite mud mixed with seawater, weight 8.8 lbs/gal or 1.11 kg/m^3) was pumped through the drill pipe to the bottom of the hole to clear the hole of debris. The bottom-hole assembly was pulled up to a depth between 60 and 100 mbsf, and then it was run down to the bottom of the hole again to ream borehole irregularities. The hole was subsequently filled with a sepiolite-seawater mud mixture, and the pipe was raised to 60–100 mbsf. Tool strings composed of one or more sensors attached to a 7-conductor wireline cable were then lowered into the hole during sequential logging runs. A wireline heave-motion compensator was employed to minimize the effect of ship's heave on the tool motion in the borehole.

During each logging run, incoming data were acquired, recorded on disk and monitored in real time on the Maxis 500 logging computer. The Cyber Service Unit (CSU) computer was used for logging with the geochemical tool string and with the well seismic tool. After logging, data were transferred to shipboard computers for preliminary interpretation.

With respect to previous ODP legs, several new logging strings and operations were implemented during Leg 166. In particular, we deployed a new logging string, the Integrated Porosity Logging Tool (IPLT; all tool acronyms are a mark of Schlumberger), and included the Schlumberger inclinometer and accelerometer sensors in the sonic tool strings to monitor tool motion and correct the logging depths for departures from the cable speed measured at the surface. In addition, we deployed a satellite communication dish on the heli-deck of the *JOIDES Resolution*, and the logging data were beamed to shore soon after logging for preliminary processing at LDEO-BRG. The processed logging data were then sent back to the ship. This experimental data transfer and processing operation represented a test case to evaluate the benefits of near real-time data processing.

Logging Tool Strings

Individual tools were combined into logging strings (Fig. 11) that were deployed in separate runs into the hole. In this manner, several measurements could be made simultaneously during a single logging run. The arrangement of logging strings varied from hole to hole, and not all strings were run in all holes. Refer to the individual site chapters for details of logging strings used at each site.

The depth of investigation into the formation and vertical resolution are sensor-dependent, but are typically between 50 and 100 cm (Table 6). The sampling interval of Schlumberger tools is usually 15 cm (6 in), with the exception of the FMS, which is 0.25 cm (0.1 in). When logged at reduced speeds, the sampling interval in the porosity and density tools can be reduced (Table 6). This high-resolution mode was enabled in all logging runs with the porosity and density tools. Special processing algorithms are used for the porosity, density, and resistivity tools, taking advantage of reduced sampling rates and multiple sensors with different spacings, which help to enhance the vertical resolution of these logs (Allen et al., 1988).

Below, we present a description of the logging tools employed during Leg 166. Further details can be obtained in the books of Serra (1984), Timur and Toksöz (1985), Ellis (1987), and Schlumberger (1989).

Logging Tools

Natural Gamma-Ray Tools

Natural gamma radiation in sedimentary formations results primarily from the unstable isotopes of potassium, thorium, and uranium and its daughter products. By counting gamma rays at different energy levels, that is, by measuring the gamma-ray spectrum, one can estimate the concentration of the three different elements by assuming that the proportion of stable and unstable isotopes is in natural equilibrium.

Two different gamma-ray tools were employed: the natural gamma-ray tool (NGT) and the hostile-environment natural gamma-ray sonde (HNGS). The NGT employs a sodium iodide (NaI) crystal that is 30 cm (12 in) tall and counts gamma rays in five energy windows. The new HNGS employs bismuth-germanate (BGO) crystals and reports gamma-ray counts in 256 energy levels. Although BGO crystals have less spectral resolution, a worse response with increasing temperature, and slightly lower counting efficiency than NaI crystals, they are more rugged and have higher gamma-ray stopping power, which decreases scattering within the crystal. To counteract the deficiencies of BGO, the HNGS tool contains two 30-cm crystals that are housed in a vacuum chamber to stabilize the internal temperature (dewar). Schlumberger's literature reports that the HNGS produces more accurate estimations of K, Th, and U than the NGT.

Geochemical Tool String

The geochemical logging tool string consists of four logging tools: the natural gamma-ray tool (NGT), the compensated neutron tool (CNT), the aluminum activation clay tool (AACT), and the gamma-ray spectrometry tool (GST; Fig. 11). The natural gamma-ray tool is located at the top of the tool string, so that it can measure the naturally occurring radio nuclides, Th, U, and K, before the formation is irradiated by the nuclear sources contained in the other tools. The compensated neutron tool, located below the natural gamma-ray tool, carries low-energy californium-252 (^{252}Cf) to activate the Al atoms in the formation (2 MeV neutrons). The aluminum activation clay tool, a modified NGT, is located below the ^{252}Cf source, measuring the activated gamma rays in the formation. By combining the AACT measurement with the previous NGT measurement, the background radiation is subtracted out and a reading of formation Al is obtained (Scott and Smith, 1973). The gamma-ray spectrometry tool (GST), at the base of the string, carries a pulsed neutron generator (14 MeV neutrons) to bombard the borehole and formation and an NaI(Tl) scintillation detector, which measures the spectrum of gamma rays generated by neutron-capture reactions. Because each of the elements in the formation is characterized by a unique spectral signature, it is possible to derive the contribution (or yield) of each of the major elements silicon (Si), iron (Fe), calcium (Ca), titanium (Ti), sulfur (S), gadolinium (Gd), and potassium (K) to the measured spectrum and, in turn, to estimate its abundance in the formation. The GST also measures the hydrogen (H) and chlorine (Cl) in the borehole and formation, but the signal for these elements is almost entirely due to seawater in the borehole, and hence they are of little value.

The only major rock-forming elements not measured by the geochemical tool string are magnesium (Mg) and sodium (Na); the neutron-capture cross-sections of these elements are too small rela-

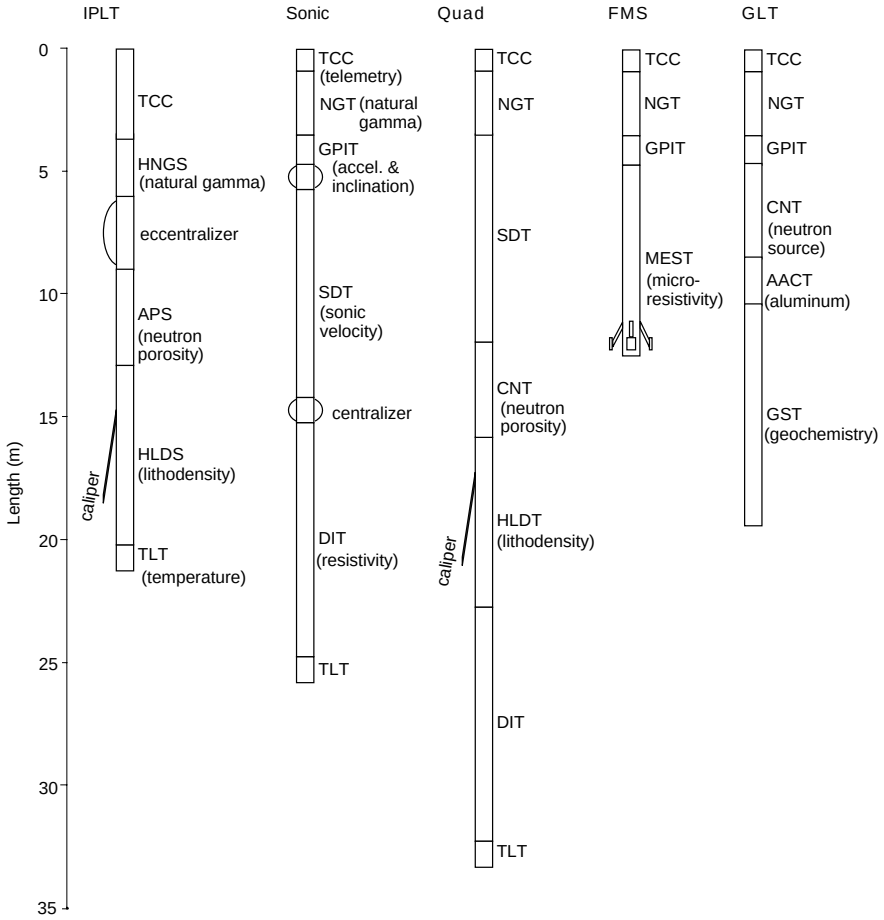

Figure 11. Configuration of tool strings deployed during Leg 166. Tool vertical dimensions are to scale. See Table 6 for acronyms.

tive to their typical abundance for the tool string to detect them. A rough estimate of Mg + Na can be made by using the photoelectric factor (PEF), measured by the lithodensity tool. This measured PEF is compared with a calculated PEF (a summation of the PEF from all of the measured elements). The separation between the measured and calculated PEF is, in theory, attributable to any element left over in the formation (i.e., Mg and Na). Further explanation of this technique is found in Hertzog et al., (1987). This Mg + Na calculation was not performed for any of the logs discussed here because of the high variance in the data resulting from poor hole conditions.

Interpretation of the geochemical logs is aided by X-ray fluorescence (XRF) analyses of the major and trace element chemistry of core samples (see "XRF Analysis" in the "Inorganic Geochemistry" section, this chapter).

Phasor Dual Induction (DIT-E) and Spherically Focused Resistivity (SFL) Tool

This tool provides three measurements of electrical resistivity, each with a different depth of investigation and vertical resolution (Table 6). These are deep induction (IDPH), medium induction (IMPH), and shallow spherically focused resistivity (SFL). The two induction devices transmit high-frequency alternating currents through transmitter coils, creating a magnetic field that induces secondary currents in the formation. These currents produce a new inductive signal, proportional to the conductivity of the formation, that is measured by the receiving coils. The measured conductivities are then converted to resistivity (in units of Ωm). The SFL measures the current necessary to maintain a constant voltage drop across a fixed interval, and is a direct measurement of resistivity.

Formation MicroScanner (FMS)

The Formation MicroScanner (FMS) produces high-resolution images of the microresistivity character of the borehole wall. This tool comprises four orthogonal pads with 16 button electrodes (each 6.7 mm in diameter) on each pad that are pressed against the borehole wall (Serra, 1989). The electrodes are arranged in two diagonally offset rows of eight electrodes each. Each pad measures about 8 cm^2, and one pass of the tool covers approximately 30% of a 25-cm diameter borehole. Each individual electrode emits a focused current into the formation. The current intensity measurements in each button are converted to variable intensity color images that reflect microresistivity variations. Processing corrects the offset rows to one level providing a vertical resolution of approximately 0.5 cm and a sampling interval of 0.25 cm (Serra, 1989). The FMS string contains a general purpose inclinometry tool (GPIT) that orients the resistivity measurements through the use of a three-axis accelerometer and a three-axis magnetometer.

General Purpose Inclinometry Tool (GPIT)

During Leg 166, we placed the GPIT in the sonic, Quad combination, and geochemical tool strings to calculate the displacement of the

Table 6. Specification of tool strings and tools deployed during Leg 166.

Tool string	Typical speed (m/hr)	Tool	Aim of measurement	Sampling interval (cm)	Approximate vertical resolution (cm)
IPLT	250–275	HNGS	Natural gamma	15	45
		APS	Porosity	3 or 15	30 or 45
		HLDS	Bulk density	5 or 15	10 or 45
		TLT*	Temperature	1/s	
Sonic	250–275	NGT	Natural gamma	15	45
		GPIT	Acceleration	0.25	0.5
		SDT	Sonic velocity	15	120
		DIT-E	Resistivity	15	75/150/200
		TLT*	Temperature	1/s	(shallow, medium, deep)
Quad combo	250–275	NGT	Natural gamma	15	45
		GPIT	Acceleration	0.25	0.5
		SDT	Sonic velocity	15	120
		CNT	Porosity	5 or 15	30 or 45
		HLDT	Bulk density	5 or 15	10 or 45
		DIT	Resistivity	15	75/150/200
		TLT*	Temperature	1/s	
FMS	500–550	NGT	Natural gamma	15	45
		GPIT	Orientation and acceleration	0.25	0.5
		MEST	Micro-resistivity	0.25	0.5
GLT	150–200	NGT	Natural gamma	15	45
		GPIT	Acceleration	0.25	0.5
		CNT	Carrier of ^{252}Cf	N/A	N/A
		AACT	Aluminum	15	60
		GST	Ca, Cl, Si, Fe, H, S	15	60
		TLT*	Temperature	1/s	
VSP	Stationary	WST	Traveltime sources (in^3)	50 m	N/A
			water-gun (80)		
			water-gun (200)		
			air-gun (120)		

Notes: * = not present in all deployments of this tool string. Tool acronyms are as follows: IPLT = integrated porosity lithology, FMS = Formation MicroScanner, VSP = vertical seismic profile. AACT = aluminum activation clay tool, APS = accelerator porosity sonde, CNT = compensated neutron tool, DIT = dual induction tool, DLL = dual latero-log, GLT = geochemical logging tool, GST = gamma-ray spectroscopy tool, HLDT = hostile environment litho-density tool, HNGS = hostile environment natural gamma tool, LDS = litho-density sonde, MEST = microelectrical resistivity scanning tool, NGT = natural gamma-ray tool, SDT = sonic digital tool (array sonic tool), TLT = temperature logging tool, GPIT = general purpose inclinometry tool, WST = well seismic tool, and a telemetry cartridge (TCC) is placed at the top of the tool string to control data transmission to/from the surface.

tool during logging using the acceleration measurements. Although a constant cable speed was maintained during logging and the effect of ship's heave on the tool motion was decreased by a wireline heave compensator, the use of the GPIT on all tool strings allowed for more precise determination of logging depths and the correction of measurements during post-cruise processing of the logs.

Neutron Porosity Tools (CNT-G and APS)

Neutron porosity tools have a source of neutrons and neutron detectors at various positions within the sonde. In the compensated neutron tool (CNT-G), a 16 Curie americium-beryllium (AmBe) source emits neutrons at an energy of 4.5 MeV. In the accelerator porosity sonde (APS), a minitron produces fast neutrons with 14 MeV. The measurement principle is the same in both tools; neutrons are slowed as they collide with nuclei of atoms surrounding the tool. The highest energy loss occurs when neutrons collide with hydrogen nuclei, which have practically the same mass as the neutron. Upon reaching thermal energies (0.025 eV), the neutrons are captured by the nuclei of chlorine, silicon, boron, and other elements, resulting in a gamma-ray emission. Neutron detectors count the number of neutrons arriving at various distances from the source. If the hydrogen concentration is small, as in low porosity formations, neutrons can travel farther before being captured, and the count rates increase at the detector. The opposite effect occurs when the water content is high.

The compensated neutron tools contain dual detectors, placed at different distances from the source. The degrading effect of borehole irregularities and tool standoff has a differential effect on the detectors. By taking the ratio of counts from each detector, the effect of tool standoff is reduced, and a compensated porosity measurement is obtained. In the CNT-G, there are two pairs of detectors, one for detecting thermal neutrons (0.025 eV) and one for epithermal neutrons (>~0.4 eV).

With the APS tool, a recent technologic advancement, more accurate porosities are determined by counting neutrons in five detectors, four epithermal and one thermal, and by using a pulsed source of high-energy neutrons (Scott et al., 1994). This new configuration provides several advantages with respect to the CNT-G. The new source is safer and has a higher neutron yield, allowing for epithermal measurements that are less sensitive to lithologic effects on neutron porosity, such as those resulting from the presence of shales and dolomites. A higher neutron yield, combined with better wall contact due to an additional eccentralizing bow-spring, reduces the effects of borehole irregularities. In addition, the pulsing of the neutron source provides for two new measurements: (1) an epithermal neutron slowdown time that is used to evaluate the tool standoff from the borehole wall and correct the porosity measurement; and (2) a formation thermal neutron cross-section (sigma) that is a useful indicator for the presence of elements of high thermal neutron capture cross-section, such as B, Cl, and rare earth elements (REEs) commonly associated with shales and possibly dolomites. The APS provides two epithermal porosity measurements: one is corrected for borehole conditions and tool standoff and is nearly independent of lithology effects, whereas the other is similar to that obtained from the CNT-G.

Lithodensity Tools (HLDT and HLDS)

The lithodensity tool uses a ^{137}Cs source of gamma-rays and two gamma-ray detectors mounted on a shielded sidewall skid that is pressed against the formation by a hydraulically activated arm. The

arm also provides a measurement of borehole diameter. The HLDS is essentially the same sonde as the HLDT, but it has improved electronics that are adapted to run in combination with the HNGS and APS of the integrated porosity-lithology tool string.

The medium energy gamma rays emitted by the source (662 keV) lose energy by interaction with the electrons in the formation by Compton scattering until absorbed through the photoelectric effect. The number of gamma rays reaching the two vertically spaced detectors yields an energy spectrum for each detector that is directly related to the number of electrons in the formation, which in turn is related to the bulk density.

Photoelectric absorption occurs when the gamma rays reach a low energy (<150 keV) after being continually scattered by electrons in the formation. As the photoelectric effect (PEF) depends on the atomic number of the elements in the formation, the magnitude of this measurement is nearly independent of porosity. The PEF values, when used in combination with other logs, can provide an indication of the different types of minerals in the sediments.

Digital Sonic Tool (SDT)

The SDT, also known as the array sonic tool, measures the time required for sound to travel through the formation between a transmitter and a receiver. As it averages replicate measurements, it provides a direct measurement of sound velocity through sediments that are relatively free from the effects of formation damage and an enlarged borehole (Schlumberger, 1989). The tool was run with centralizer sections placed both above and below the tool, except for the logging run with the Quad combo string in Hole 1007C.

The SDT contains two broadband piezoelectric ceramic transmitters spaced 61 cm apart and two piezoelectric receivers spaced 61 cm apart with the lower receiver located 91 cm above the upper transmitter. In addition, eight wideband ceramic receivers are arranged in an array 1.07 m long, 2.44 m above the upper transmitter at the base of the sonde. This configuration provides a total of eight different transit time measurements. Interval transit times are converted to compressional-wave velocities (km/s). Full waveforms are recorded by the tool, allowing shore-based post-processing to estimate shear and Stoneley wave velocities, as well as amplitude attenuation. Logs are edited for cycle-skipping and obvious bad values.

Well Seismic Tool (WST) and Time vs. Depth Calibration

The WST consists of a single geophone pressed against the borehole wall that is used to record the acoustic waves generated by an air gun located near the sea surface. We employed a 120-in^3 air gun suspended by buoys at a depth of 3 mbsl, offset 48.5 m from the hole on the port side. The WST was clamped against the borehole wall at intervals of approximately 50 m, and the air gun fired five to seven times. The resulting waveforms were stacked and a traveltime determined from the median of the first breaks in each trace. This "check shot" experiment attempts to reproduce the seismic reflection profiling by simulating a similar geometry and source frequency. In general, the acoustic velocities, and resulting depth-traveltime pairs, determined from the sonic tool differ significantly from the seismic velocities because of frequency dispersion (e.g., the sonic tool works at 10–20 kHz vs. 50–100 Hz in seismic data) and because the sound is forced to travel along the borehole wall, a path that is quite different from the one taken by the air gun signal generated during a seismic reflection survey. In addition, sonic logs are not obtained above the bottom-hole assembly, and the traveltime to the uppermost logging point has to be estimated by some other means.

The WST was deployed in all logged holes and measurement stations occupied every ~50 m. Depth-traveltime pairs determined from the check shots were used to produce a depth-traveltime move and to calibrate the sonic logs and determine accurate drilling depths and their relative position with respect to targets on the seismic reflection profiles.

Lamont-Doherty Temperature Tool (LDEO-TLT)

This high-precision, low-temperature, self-recording logging tool was attached to the bottom of the Schlumberger tool strings (Fig. 11). Data are recorded as a function of time, with conversion to depth based on a synchronized time-cable depth record. We deployed the TLT in the first logging run of each hole and also in the second run in Holes 1005A and 1005C.

Data Processing

Preliminary editing, processing, display, and interpretation of the logging data were performed aboard the ship. Final corrections for environmental effects, editing, and depth correlation between runs will be performed post-cruise. During Leg 166, we processed the logging data in near-real time and performed the depth shifting necessary to match the logs from different runs by transmitting the data to the LDEO processing center via satellite (using a Ku band proprietary communications system provided by OMNIS, a division of Schlumberger). After processing, the data were beamed back to the ship and made available to the scientific party.

Processing, quality control, and display of the logging data were performed at each of the five holes logged during Leg 166 by the Borehole Research Group (BRG) at LDEO, the Institut Mediterraneén de Technologie, and Schlumberger GeoQuest using Schlumberger "Logos" software and additional programs developed by members of the BRG. Displays of most of these processed data appear with accompanying text at the end of the appropriate site chapters in this volume. Files of all processed logs (including FMS, dipmeter, temperature data, high-resolution density and neutron data, and sonic data are not shown in printed form) and explanatory text are included on CD-ROM enclosed in the back pocket of this volume; a directory of the contents of the CD is found in the table of contents for this volume.

Shore-based processing of data from each hole consisted of: (1) depth adjustments of all logs to a common measurement below the seafloor; (2) corrections specific to certain tools; and (3) quality control and rejection of unrealistic values.

The depth-shifting procedure is based on an interactive, graphical depth-match program that allows the processor to visually correlate logs and define appropriate shifts. The reference log and the log to be adjusted in depth are displayed side-by-side on a screen, and vectors connect the two at positions chosen by the user. The total gamma-ray from the NGT (SGR curve) or HNGS (HSGR curve) tool run on each logging string was used in most cases to correlate the logging runs. In general, the reference curve is chosen on the basis of constant, low cable tension and high cable speed (tools run at faster speeds are less likely to stick and are less susceptible to data degradation caused by ship heave). Other factors, however, such as the length of the logged interval, position of the bottom-hole assembly, and the statistical quality of the collected data (better statistics are obtained at lower logging speeds) are also considered in the selection. A list of the amount of differential depth shifts applied at each hole is available upon request to LDEO-BRG.

Specific tool corrections were performed on the gamma-ray data (NGT) to account for changes in borehole size and for the composition of the drilling fluid. The HNGS data are corrected in real time during the recording. Processing techniques unique to the AACT and GST tools of the geochemical string are described in detail below.

Quality control was performed by cross-correlation of all logging data. If the data processor concluded that individual log measurements represented unrealistic values, the choices were to either discard the data outright and substitute the null value of "–999.25," or

identify a specific depth interval containing suspect values that must be used with caution. The latter are noted in the text that accompanies all processed log displays at the end of individual site chapters. Quality control of the acoustic data was based on discarding any of the four independent transit time measurements that were negative or that fell outside a range of reasonable values.

In addition to the standard 15.24 cm sampling rate, bulk density (HLDT tool) and neutron data (APS tool) were recorded at a sampling rate of 2.54 and 5.08 cm, respectively. HLDT high-resolution data were collected at Hole 1007C only; due to a software problem, no high-resolution bulk-density data were recorded with the HLDS from the new IPLT string in the remaining holes. The enhanced bulk density curve is the result of the Schlumberger-enhanced processing technique performed on the MAXIS system on board. In normal processing, short-spacing data are smoothed to match the long-spacing ones, but in enhanced processing, this is reversed. Where there is good contact between the HLDT pad and the borehole wall (small density correction), the results are improved, because the short-spacing data have better vertical resolution.

Locally, some intervals of log data appeared unreliable (usually due to poor hole conditions) and were not processed. In general, a large (>12 in) and/or irregular borehole affects most recordings, particularly those that require eccentralization (HLDT, HLDS, APS) and a good contact with the borehole wall. Hole deviation can also degrade the data; the FMS, for example, is not designed to be run in holes that are more than 10° off the vertical, as the tool weight might cause the caliper to close.

Processing of Geochemical Logging Data[3]

The well log data from the Schlumberger tools are transmitted digitally up a wireline and are recorded on the *JOIDES Resolution* in the Schlumberger Cyber Service Unit (CSU). The results from the CSU are made available as "field logs" for initial, shipboard interpretation. Subsequent reprocessing is necessary to correct the data for the effects of fluids added to the well, logging speed, and pipe interference. Processing of the spectrometry data is required to transform the relative elemental yields into oxide weight fractions.

The processing is performed with a set of log interpretation programs written by Schlumberger that have been slightly modified to account for the lithologies and hole conditions encountered in ODP holes. The processing steps are summarized below.

Step 1: Reconstruction of relative elemental yields from recorded spectral data

The first processing step uses a weighted least-squares method to compare the measured spectra from the geochemical spectroscopy tool with a series of standard spectra to determine the relative contribution (or yield) of each element. Six elemental standards (Si, Fe, Ca, S, Cl, and H) are used to produce the shipboard yields; three additional standards (Ti, Gd, and K) are included in the shore-based processing to improve the fit of the spectral standards to the measured spectra (Grau and Schweitzer, 1989). Although these additional elements often appear in the formation in very low concentrations, they can make a large contribution to the measured spectra, because they have large neutron-capture cross-sections. For example, the capture cross-section of Gd is 49,000 barns; that of Si is 0.16 barns (Hertzog et al., 1987). Gd is, therefore, included in the calculation of a best fit between the measured and the standard spectra. This best-fit analysis was done for the elements in Hole 1003D to include spectral standards for Si, Ca, Gd, H, and Cl. The exclusion of Fe, Ti, S, and K from the best-fit analysis was decided in order to improve the quality of the Ca estimate; in fact, sediments at this hole consist largely of carbonates, with $CaCO_3$ concentrations up to 90%. Although sulfur was present in Hole 1003D sediments, its concentration was below the resolution of the geochemical tool.

Step 2: Depth-shifting

The second step in log processing is to depth shift the logging runs to a chosen reference run. A total gamma-ray curve (from the NGT, which is run on each tool string) is usually chosen as a reference curve, based on cable tension (the logging run with the least amount of cable sticking) and cable speed (tools run at faster speeds are less likely to stick). For Hole 1003D, the depth reference run was taken from the APS/HLDS/HNGS run.

Step 3: Calculation of total radioactivity and Th, U, and K concentrations

The third processing routine calculates the total natural gamma radiation in the formation as well as concentrations of Th, U, and K, using the counts in five spectral windows from the natural gamma-ray tool (Lock and Hoyer, 1971), including corrections for hole-size changes. A Kalman filter (Ruckebusch, 1983) was applied to minimize the statistical uncertainties in the logs, which would otherwise create erroneous negative readings and anti-correlation (especially between Th and U). At each depth level, calculations and corrections also were performed for K contained in the mud. The outputs of this program are: K (wet wt%), U (ppm), and Th (ppm), along with a total gamma-ray curve (SGR) and a computed gamma-ray curve (CGR, total gamma ray minus U contribution).

Step 4: Calculation of Al concentration

The fourth processing routine calculates an Al curve using four energy windows, while concurrently correct for natural activity, borehole fluid neutron-capture cross-section, formation neutron-capture cross-section, formation slowing-down length, and borehole size. Porosity and density logs are needed in this routine to convert the wet weight percent K and Al curves to dry weight percent.

A correction is also made for Si interference with Al; the ^{252}Cf source also activates Si, producing the aluminum isotope, ^{28}Al (Hertzog et al., 1987). The program uses the Si yield from the gamma-ray spectrometry tool to determine the Si background correction. The program outputs dry weight percentages of Al and K, which are used in the calculation and normalization of the remaining elements.

Step 5: Normalization of elemental yields from the GST to calculate the elemental weight fractions

This routine combines the dry weight percentages of Al and K with the reconstructed yields to obtain dry weight percentages of the GST elements using the relationship

$$W_i = F\, Y_i / S_i, \tag{9}$$

where

W_i = dry weight percentage of the i-th element,
F = normalization factor determined at each depth interval,
Y_i = relative elemental yield for the i-th element, and
S_i = relative weight percentage (spectral) sensitivity of the i-th element.

The normalization factor, F, is a calibration factor determined at each depth from a closure argument to account for the number of neutrons captured by a specific concentration of rock elements. Because the sum of oxides in a rock is 100%, F is given by

$$F\,(\sum X_i\, Y_i / S_i) + X_K\, W_K + X_{Al}\, W_{Al} = 100.0, \tag{10}$$

[3]Performed by Elizabeth L. Pratson at Schlumber GeoQuest, 6090 Greenwood Plaza, Englewood, CO 80111, U.S.A.

where

X_i = factor for the element to oxide (or carbonate) conversion,
X_K = factor for the conversion of K to K_2O (1.205),
X_{Al} = factor for the conversion of Al to Al_2O_3 (1.899),
W_K = dry weight percentage of K determined from natural activity, and
W_{Al} = dry weight percentage of Al determined from the activation measurement.

The sensitivity factor, S_i, is a tool constant measured in the laboratory, that depends on the capture cross-section, gamma-ray production, and detection probabilities of each element measured by the GST (Hertzog et al., 1987). The factors X_i are simply element to oxide (or carbonate, sulfate, etc.) conversion coefficients and effectively include the O, C, or S bound with each element. In processing the GLT data, the correct choice of X_i is important in the closure algorithm described above and requires some geological input. In most lithologies the elements measured by the tool occur in silicates where the compositions can be expressed completely as oxides. In carbonate lithologies the measured calcium is more likely to be present as $CaCO_3$ (X_{Ca} = 2.497) than as the oxide (CaO; X_{Ca} = 1.399). A good indication of the choice of calcium conversion factors can often be gained from shipboard X-ray diffraction (XRD) and $CaCO_3$ measurements. In the absence of suitable shipboard data a rough rule of thumb is generally used such that, if elemental Ca is below 6%, then all Ca is assumed to be in silicate, above 12%, in carbonate. Ca concentrations between these figures are converted using linear interpolation. The variable Ca oxide factor was not used in the remaining of Hole 1003D data.

Step 6: Calculation of oxide percentages

This routine converts the elemental weight percentages into oxide percentages by multiplying each by its associated oxide factor, as shown in Table 7. The results are displayed as a function of depth in the log summary figures at the end of the relevant site chapter (this volume); the calcium carbonate measurements performed on board for all three holes (1003A, 1003B, and 1003C) are also displayed.

Step 7: Calculation of error logs

The seventh and final step in processing is the calculation of the statistical uncertainty of each element, using methods described by Grau et al. (1990) and Schweitzer et al. (1988). This error is strongly related to the normalization factor, *F*, which is calculated at each depth level. Both normalization factor and statistical uncertainties are displayed as a function of depth in the log summary figures at the end of the relevant site chapter (this volume). A lower normalization factor represents better counting statistics and therefore higher quality data.

IN SITU TEMPERATURE MEASUREMENTS

In situ temperature measurements were made with two types of instruments: the "Adara tool" and the Water Sampling Temperature Probe (WSTP).

Table 7. Oxide factors used in normalizing elements to 100% and converting elements to oxides.

Element	Oxide/carbonate	Conversion factor
Si	SiO_2	2.139
Ca	$CaCO_3$	2.497
K	K_2O	1.205
Al	Al_2O_3	1.889

The Adara tool is housed entirely inside the coring shoe of the advanced piston corer (APC). In a normal deployment, the tool first stops briefly at the mudline before entering the borehole and thermally equilibrates with the bottom water. After the APC penetrates to the bottom sediments, it is held there for about 10 min and records the temperature of the cutting shoe every 5 s. As a result of the frictional heating caused by the APC penetration, the temperature rises instantaneously, but decreases gradually as the heat dissipates to the surrounding sediments. One can theoretically extrapolate the equilibrium temperature of the sediment by applying a mathematical heat conduction model to the temperature decay record (Horai and Von Herzen, 1985). More technical information of the instrument can be found in the Legs 139 and 150 *Initial Reports* volumes (Shipboard Scientific Party, 1992, 1994b)

The second type of instrumentation, WSTP, is used for semilithified sediments that are too hard for the APC to penetrate. The schematic diagram of the mechanical configuration of the WSTP is shown in the Leg 139 *Initial Reports* volume (Shipboard Scientific Party, 1992). The WSTP consists of three cylindrical parts with different diameters. The lowermost part is a metal tube 1.3 cm in diameter and 5.5 cm in length that contains a thermistor. The second part is normally the water sampler, which is 2.7 cm in diameter and 25 cm in length, but for Leg 166 it was replaced with a solid rod of the same dimensions, because no water samples were collected during Leg 166. The third part, the housing for the data logger and the batteries, is 6 cm in diameter and ~85 cm in length.

Unlike the Adara tool, the WSTP requires a separate wireline run. It is mounted inside the core barrel and lowered down the drill pipe by wireline while the bit is held above the bottom of the hole. It stops briefly at the mudline, equilibrates with the bottom water, and then is pushed into the undisturbed bottom sediments. The thermal response at the penetration of the WSTP is similar to that of the APC, but the reduction of the data is simpler because of its geometrical configuration. In fact, the data can be processed in a way similar to those of the modern marine heat flow probe (Villinger and Davis, 1987; Nagihara and Lister, 1993).

Water depths of the Leg 166 sites were among the shallowest in which these tools had ever been deployed, and therefore we took special care to deal with some of the operational problems associated with the shallow-water deployment, especially in regard to the Adara tool. In a normal deployment in deeper (>2000 m) water, the mudline stop can be very short (less than 5 min) because the thermal gradient of the bottom water is near zero and the APC is already approaching thermal equilibrium during the long descent. In shallow water, however, temperature continues to decrease all the way down to the bottom. The time between the surface deployment and the mudline stop is very short. In addition, the water circulated within the drill pipe can be several degrees warmer than the ambient bottom water, though the circulation pump is usually shut off just before the mudline stop. Therefore, it takes about 10 min before the APC shoe thermally equilibrates with the bottom water at the mudline. This problem is less serious with the WSTP because it has a heat capacity and a thermal time constant much lower than the Adara temperature shoe.

REFERENCES

Allen, D., Barber, T., Flaum, C., Hemingway, J., Anderson, B., des Ligneris, S., Everett, B., and Morriss, C., 1988. Advances in high-resolution logging. *Tech. Rev.*, 36:4–15.

ASTM, 1989. *Annual Book of ASTM Standards for Soil and Rock: Building Stones* (Vol. 4.08): *Geotextiles:* Philadelphia (Am. Soc. Testing and Mater.).

Berggren, W.A., Hilgen, F.J., Langereis, C.G., Kent, D.V., Obradovich, J.D., Raffi, I., Raymo, M.E., and Shackleton, N.J., 1995a. Late Neogene chronology: new perspectives in high-resolution stratigraphy. *Geol. Soc. Am. Bull.*, 107:1272–1287.

Berggren, W.A., Kent, D.V., Swisher, C.C., III, and Aubry, M.-P., 1995b. A revised Cenozoic geochronology and chronostratigraphy. *In* Berggren,

W.A., Kent, D.V., Aubry, M.-P., and Hardenbol, J. (Eds.), *Geochronology, Time Scales and Global Stratigraphic Correlation.* Spec. Publ.—Soc. Econ. Paleontol. Mineral., 54:129–212.

Blow, W.H., 1969. Late middle Eocene to Recent planktonic foraminiferal biostratigraphy. *In* Brönnimann, P., and Renz, H.H. (Eds.), *Proc. First Int. Conf. Planktonic Microfossils, Geneva, 1967:* Leiden (E.J. Brill), 1:199–422.

Boyce, R.E., 1976. Definitions and laboratory techniques of compressional sound velocity parameters and wet-water content, wet-bulk density, and porosity parameters by gravimetric and gamma-ray attenuation techniques. *In* Schlanger, S.O., Jackson, E.D., et al., *Init. Repts. DSDP,* 33: Washington (U.S. Govt. Printing Office), 931–958.

————, 1977. Deep Sea Drilling Project procedures for shear strength measurement of clayey sediment using modified Wykeham Farrance laboratory vane apparatus. *In* Barker, P.F., Dalziel, I.W.D., et al., *Init. Repts. DSDP,* 36: Washington (U.S. Govt. Printing Office), 1059–1068.

Cande, S.C., and Kent, D.V., 1995. Revised calibration of the geomagnetic polarity timescale for the Late Cretaceous and Cenozoic. *J. Geophys. Res.*, 100:6093–6095.

Chaisson, W.P., and Pearson, P.N., in press. Planktonic foraminifer biostratigraphy at Site 925, western tropical Atlantic: the last 12 m.y. *In* Shackleton, N.J., Curry, W.B., Richter, C., and Bralower, T.J., (Eds.) *Proc. ODP, Sci. Results,* 154: College Station (Ocean Drilling Program).

Curry, W.B., Shackleton, N.J., Richter, C., et al., 1995. *Proc. ODP, Init. Repts.*, 154: College Station, TX (Ocean Drilling Program).

Dunham, R.J., 1962. Classification of carbonate rocks according to depositional texture. *In* Ham, W.E. (Ed.), *Classification of Carbonate Rocks.* AAPG Mem., 108–121.

Ellis, D.V., 1987. *Well Logging for Earth Scientists:* New York (Elsevier).

Embry, A.F., and Klovan, J.E., 1971. A late Devonian reef tract on northeastern Banks Island, Northwest Territories. *Bull. Can. Pet. Geol.,* 19:730–781.

Emeis, K.-C., and Kvenvolden, K.A., 1986. Shipboard organic geochemistry on *JOIDES Resolution. ODP Tech. Note,* 7.

Espitalié, J., Deroo, G., and Marquis, F., 1986. La pyrolyse Rock-Eval et ses applications, Partie III. *Rev. Inst. Fr. Pet.,* 41:73–89.

Froelich, P.N., Kim, K.H., Jahnke, R., Burnett, W.C., Soutar, A., and Deakin, M., 1983. Pore water fluoride in Peru continental margin sediments: uptake from seawater. *Geochim. Cosmochim. Acta,* 47:1605–1612.

Gealy, E.L., Winterer, E.L., and Moberly, R., Jr., 1971. Methods, conventions, and general observations. *In* Winterer, E.L., Riedel, W.R., et al., *Init. Repts. DSDP,* 7 (Pt. 1): Washington (U.S. Govt. Printing Office), 9–26.

Gieskes, J.M., Gamo, T., and Brumsack, H., 1991. Chemical methods for interstitial water analysis aboard *JOIDES Resolution. ODP Tech. Note,* 15.

Grau, J.A., and Schweitzer, J.S., 1989. Elemental concentrations from thermal neutron capture gamma-ray spectra in geological formations. *Nucl. Geophys.*, 3:1–9.

Grau, J.A., Schweitzer, J.S., and Hertzog, R.C., 1990. Statistical uncertainties of elemental concentrations extracted from neutron-induced gamma-ray measurements. *IEEE Trans. Nucl. Sci.*, 37:2175–2178.

Hagelberg, T., Shackleton, N., Pisias, N., and Shipboard Scientific Party, 1992. Development of composite depth sections for Sites 844 through 854. *In* Mayer, L., Pisias, N., Janecek, T., et al., *Proc. ODP, Init. Repts.*, 138 (Pt. 1): College Station, TX (Ocean Drilling Program), 79–85.

Hertzog, R.C., Colson, J.L., Seeman, B., O'Brien, M.S., Scott, H.D., McKeon, D.C., Wraight, P.D., Grau, J.A., Ellis, D.V., Schweitzer, J.S., and Herron, M.M., 1987. Geochemical logging with spectrometry tools. *Soc. Pet. Eng. Pap.*, 16792.

Hooton, D.H., and Giorgetta, N.E., 1977. Quantitative x-ray diffraction analysis by a direct calculation method. *X-Ray Spectrom.*, 6:2–5.

Horai, K., and Von Herzen, R.P., 1985. Measurement of heat flow on Leg 86 of the Deep Sea Drilling Project. *In* Heath, G.R., Burckle, L.H., et al., *Init. Repts. DSDP,* 86: Washington (U.S. Govt. Printing Office), 759–777.

Kennett, J.P., and Srinivasan, M.S., 1983. *Neogene Planktonic Foraminifera: A Phylogenetic Atlas:* Stroudsburg, PA (Hutchinson Ross).

Kvenvolden, K.A., and McDonald, T.J., 1986. Organic geochemistry on the *JOIDES Resolution*—an assay. *ODP Tech. Note,* 6.

Lloyd, J., and Moran, K., 1992. ODP GRAPE evaluation: a report to the JOIDES Shipboard Measurements Panel. *Internal Rept., Ocean Drilling Program.*

Lock, G.A., and Hoyer, W.A., 1971. Natural gamma-ray spectral logging. *Log Analyst,* 12:3–9.

Manheim, F.T., and Sayles, F.L., 1974. Composition and origin of interstitial waters of marine sediments, based on deep sea drill cores. *In* Goldberg, E.D. (Ed.), *The Sea* (Vol. 5): *Marine Chemistry: The Sedimentary Cycle:* New York (Wiley), 527–568.

Martini, E., 1971. Standard Tertiary and Quaternary calcareous nannoplankton zonation. *In* Farinacci, A. (Ed.), *Proc. 2nd Int. Conf. Planktonic Microfossils Roma:* Rome (Ed. Tecnosci.), 2:739–785.

Mazzullo, J.M., Meyer, A., and Kidd, R.B., 1988. New sediment classification scheme for the Ocean Drilling Program. *In* Mazzullo, J., and Graham, A.G. (Eds.), *Handbook for Shipboard Sedimentologists.* ODP Tech. Note, 8:45–67.

McKee, E.D., and Weir, G.W., 1953. Terminology for stratification and cross-stratification in sedimentary rocks. *Geol. Soc. Am. Bull.,* 64:381–390.

McNeill, D.F., Eberli, G.P., Lidz, B.H., Swart, P.K., and Kenter, J.A.M., in press. Chronostratigaphy of prograding carbonate platform margins: a record of dynamic slope sedimentation, Western Great Bahama Bank. *In* Ginsburg, R.N. (Ed.), SEPM Contributions in Sedimentology.

Munsell Color Company, Inc., 1992. *Munsell Soil Color Charts* (Rev. ed.): Newburgh, MD (Munsell Color Company).

Nagihara, S., and Lister, C.R.B., 1993. Accuracy of the marine heat flow instrumentation: numerical studies on probe construction and the data reduction scheme. *Geophys. J. Int.,* 112:161–177.

Peters, K.E., 1986. Guidelines for evaluating petroleum source rock using programmed pyrolysis. *AAPG Bull.,* 70:318–329.

Ruckebusch, G., 1983. A Kalman filtering approach to natural gamma ray spectroscopy in well logging. *IEEE Trans. Autom. Control,* AC-28:372–380.

Sato, T., and Kameo, K., 1996. Pliocene to Quaternary calcareous nannofossil biostratigraphy of the Arctic Ocean, with reference to late Pliocene glaciation. *In* Thiede, J., Myhre, A.M., Firth, J.V., Johnson, G.L., and Ruddiman, W.F. (Eds.), *Proc. ODP, Sci. Results,* 151: College Station, TX (Ocean Drilling Program), 39–59.

Sato, T., Kameo, K., and Takayama, T., 1991. Coccolith biostratigraphy of the Arabian Sea. *In* Prell, W.L., Niitsuma, N., et al., *Proc. ODP, Sci. Results,* 117: College Station, TX (Ocean Drilling Program), 37–54.

Schlager, W., and James, N.P., 1978. Low-magnesian calcite limestones forming at the deep-sea floor, Tongue of the Ocean, Bahamas. *Sedimentology,* 25:675–702.

Schlumberger, 1989. *Log Interpretation Principles/Applications:* Houston, TX (Schlumberger Educ. Services).

Schweitzer, J.S., Grau, J.A., and Hertzog, R.C., 1988. Precision and accuracy of short-lived activation measurements for in situ geological analyses. *J. Trace Microprobe Techniques,* 6:437–451.

Scott, H.D., and Smith, M.P., 1973. The aluminum activation log. *Log Analyst,* 14:3–12.

Scott, H.D., Wraight, P.D., Thornton, J.L., Olesen, J.-R., Hertzog, R.C., McKeon, D.C., DasGupta, T., and Albertin, I.J., 1994. Response of a multidetector pulsed neutron porosity tool. *SPWLA 35th Ann. Logging Symp.*, Pap. XX, 1–25.

Serra, O., 1984. *Fundamentals of Well-Log Interpretation* (Vol. 1): *The Acquisition of Logging Data:* Dev. Pet. Sci., 15A: Amsterdam (Elsevier).

————, 1989. *Formation MicroScanner Image Interpretation:* Houston (Schlumberger Educ. Services), SMP-7028.

Shepard, F., 1954. Nomenclature based on sand-silt-clay ratios. *J. Sediment. Petrol.,* 24:151–158.

Shipboard Scientific Party, 1988. Site 702. *In* Ciesielski, P.F., Kristoffersen, Y., et al., *Proc. ODP, Init. Repts.,* 114: College Station, TX (Ocean Drilling Program), 483–548.

————, 1991a. Explanatory notes. *In* Davies, P.J., McKenzie, J.A., Palmer-Julson, A., et al., *Proc. ODP, Init. Repts.,* 133 (Pt. 1): College Station, TX (Ocean Drilling Program), 31–58.

————, 1991b. Site 812. *In* Davies, P.J., McKenzie, J.A., Palmer-Julson, A., et al., *Proc. ODP, Init. Repts.,* 133 (Pt. 1): College Station, TX (Ocean Drilling Program), 135–176.

————, 1991c. Site 813. *In* Davies, P.J., McKenzie, J.A., Palmer-Julson, A., et al., *Proc. ODP, Init. Repts.,* 133 (Pt. 1): College Station, TX (Ocean Drilling Program), 177–202.

————, 1992. Explanatory notes. *In* Davis, E.E., Mottl, M.J., Fisher, A.T., et al., *Proc. ODP, Init. Repts.,* 139: College Station, TX (Ocean Drilling Program), 55–97.

————, 1993. Explanatory notes. *In* Rea, D.K., Basov, I.A., Janecek, T.R., Palmer-Julson, A., et al., *Proc. ODP, Init. Repts.*, 145: College Station, TX (Ocean Drilling Program), 9–33.
————, 1994a. Explanatory notes. *In* Larsen, H.C., Saunders, A.D., Clift, P.D., et al., *Proc. ODP, Init. Repts.*, 152: College Station, TX (Ocean Drilling Program), 17–39.
————, 1994b. Explanatory notes. *In* Mountain, G.S., Miller, K.G., Blum, P., et al., *Proc. ODP, Init. Repts.*, 150: College Station, TX (Ocean Drilling Program), 21–42.
————, 1995a. Explanatory notes. *In* Curry, W.B., Shackleton, N.J., Richter, C., et al., *Proc. ODP, Init. Repts.*, 154: College Station, TX (Ocean Drilling Program), 11–38.
————, 1995b. Explanatory notes. *In* Shipley, T.H., Ogawa, Y., Blum, P., et al., *Proc. ODP, Init. Repts.*, 156: College Station, TX (Ocean Drilling Program), 39–68.
————, 1997. Explanatory notes. *In* Sigurdsson, H., Leckie, R.M., Acton, G.D., et al., *Proc. ODP, Init. Repts.*, 165: College Station, TX (Ocean Drilling Program), 15–46.
Takayama, T., and Sato, T., 1987. Coccolith biostratigraphy of the North Atlantic Ocean, Deep Sea Drilling Project Leg 94. *In* Ruddiman, W.F., Kidd, R.B., Thomas, E., et al., *Init. Repts. DSDP,* 94 (Pt. 2): Washington (U.S. Govt. Printing Office), 651–702.
Timur, A., and Toksöz, M.N., 1985. Downhole geophysical logging. *Annu. Rev. Earth Planet. Sci.*, 13:315–344.
Tissot, B.P., and Welte, D.H., 1984. *Petroleum Formation and Occurrence* (2nd ed.): Heidelberg (Springer-Verlag).
Vacquier, V., 1985. The measurement of thermal conductivity of solids with a transient linear heat source on the plane surface of a poorly conducting body. *Earth Planet. Sci. Lett.*, 74:275–279.
van Morkhoven, F.P.C.M., Berggren, W.A., and Edwards, A.S., 1986. Cenozoic cosmopolitan deep-water benthic foraminifera. *Bull. Cent. Rech. Explor.-Prod. Elf-Aquitaine*, Mem. 11.
Villinger, H., and Davis, E.E., 1987. A new reduction algorithm for marine heat flow measurements. *J. Geophys. Res.*, 92:12846–12856.
Von Herzen, R.P., and Maxwell, A.E., 1959. The measurement of thermal conductivity of deep-sea sediments by a needle-probe method. *J. Geophys. Res.*, 64:1557–1563.
Wentworth, C.K., 1922. A scale of grade and class terms of clastic sediments. *J. Geol.*, 30:377–392.

Ms 166IR-104

Previous Chapter Table of Contents Next Chapter